https://doi.org/10.5194/gmd-2019-176
Preprint. Discussion started: 27 August 2019

Geoscientific Model Development Discussions

The Vertical City Weather Generator (VCWG v1.0.0)

Mohsen Moradi[1], Benjamin Dyer[2], Amir Nazem[1], Manoj K. Nambiar[1], M. Rafsan Nahian[1], Bruno Bueno[5], Chris Mackey[7], Saeran Vasanthakumar[8], Negin Nazarian[3], E. Scott Krayenhoff[4], Leslie K. Norford[6], and Amir A. Aliabadi[1]

[1]School of Engineering, University of Guelph, Guelph, Canada
[2]Department of Physics and Astronomy, McMaster University, Hamilton, Canada
[3]Built Environment, University of New South Wales, Sydney, Australia
[4]School of Environmental Sciences, University of Guelph, Guelph, Canada
[5]Fraunhofer Institute for Solar Energy Systems ISE, Freiburg, Germany
[6]Department of Architecture, Massachusetts Institute of Technology, Cambridge, USA
[7]Ladybug Tools LLC, Boston, USA
[8]Kieran Timberlake Research Group, Philadelphia, USA

Correspondence: Amir A. Aliabadi (aliabadi@uoguelph.ca)

Abstract. The Vertical City Weather Generator (VCWG) is a computationally efficient urban microclimate model developed to predict temporal and vertical variation of temperature, wind speed, and specific humidity. It is composed of various sub models: a rural model, an urban microclimate model, and a building energy model. In a nearby rural site, a rural model is forced with weather data to solve a vertical diffusion equation to calculate vertical potential temperature profiles using a novel parameterization. The rural model also calculates a horizontal pressure gradient. The rural model outputs are then forced on a vertical diffusion urban microclimate model that solves vertical transport equations for momentum, temperature, and specific humidity. The urban microclimate model is also coupled to a building energy model using feedback interaction. The aerodynamic and thermal effects of urban elements and vegetation are considered in VCWG. To evaluate the VCWG model, a microclimate field campaign was held in Guelph, Canada, from 15 July 2018 to 5 September 2018. The meteorological measurements were carried out under a comprehensive set of wind directions, wind speeds, and thermal stability conditions in both the rural and the nearby urban areas. The model evaluation indicated that the VCWG predicted vertical profiles of meteorological variables in reasonable agreement with field measurements for selected days. In comparison to measurements, the overall model biases for potential temperature, wind speed, and specific humidity were within 5%, 11%, and 7%, respectively. The performance of the model was further explored to investigate the effects of urban configurations such as plan and frontal area densities, varying levels of vegetation, seasonal variations, different climate zones, and time series analysis on the model predictions. The results obtained from the explorations were reasonably consistent with previous studies in the literature, justifying the reliability and computational efficiency of VCWG for operational urban development projects.

1 Introduction

Urban areas interact with the atmosphere through various exchange processes of heat, momentum, and mass, which substantially impact the human comfort, air quality, and urban energy consumption. Such complex interactions are observable from

https://doi.org/10.5194/gmd-2019-176
Preprint. Discussion started: 27 August 2019

Geoscientific Model Development Discussions

the Urban Canopy Layer (UCL) to a few hundred meters within the Atmospheric Boundary Layer (ABL) (Britter and Hanna, 2003). Much of the urban climate research has focused on UCL, characterized by a heterogeneous urban structure, variety of human activities, and pollution sources. There is evidence that urban development can modify the urban climate by changing the atmosphere-earth surface interactions (Oke, 1982). It can noticeably affect atmospheric stability, dispersion of pollutants, and the Urban Heat Island (UHI), creating warmer cities than the surrounding undeveloped areas. The latter can often have significant negative influences on building energy performance and human health (Akbari, 2005). The UHI is mainly attributed to the reduction in loss of longwave radiation within the urban area, increased heat storage, anthropogenic heat released from human activities, urban greenhouse effect, inter-reflections of radiation within the surfaces of urban elements, and loss of evaporation from surfaces compared to vegetated surfaces (Oke et al., 1991), all of which affect energy performance of buildings (C. S. B. Grimmond, 2009).

UHI can be viewed as a primarily nighttime phenomenon, but it can also be occasionally observed during daytime. It has been suggested that the UHI pattern is strongly influenced by wind speed, wind direction, and the daily maximum air temperature at a rural site nearby a city (Founda and Santamouris, 2017). During extremely high temperatures, which may be accompanied by high humidity and higher absorption and storage of heat in urban areas, as opposed to rural areas, urban surfaces exhibit higher temperatures and, therefore, the sensible heat released from urban surfaces amplify (Li and Bou-Zeid, 2013; Founda and Santamouris, 2017). Daytime UHI has been reported in Hong Kong (Siu and Hart, 2013), where UHI was detected in the early afternoon and at its peak just before sunset. Most commonly during nighttime, urban areas cool down at a lower rate than the surrounding rural areas due to radiation trapping and reduced convection so that the UHI is at its maximum at nights. In addition, excessive heat gain during a heat wave will be released into the urban environment at nights with noticeable UHI (Oke, 1982; Founda and Santamouris, 2017). Nevertheless, the UHI phenomenon is more complicated to be easily generalized because it depends on multiple factors such as built density, ventilation rate, shading, radiation heat transfer, evaporation, and more, where occasionally an Urban Cool Island (UCI) can also be observed in the same climate zone (Yang et al., 2017).

Mesoscale models incorporating the urban climate were initially aimed to resolve weather features with grid resolutions of at best few hundred meters horizontally and a few meters vertically, without the functionality to resolve micro-scale three-dimensional flows or to account for atmospheric interactions with specific urban elements such as roads, roofs, and walls (Bornstein, 1975). These models usually consider the effect of built-up areas by introducing an urban aerodynamic roughness length (Grimmond and Oke, 1999) or adding source or sink terms in the momentum (drag) and energy (anthropogenic heat) equations (Dupont et al., 2004). Therefore, if higher grid resolutions less than ten meters (horizontal and vertical) are desired (Moeng et al., 2007; Wang et al., 2009; Talbot et al., 2012), microscale climate models should be deployed. Some efforts also have begun to develop multi-scale climate models by coupling mesoscale and microscale models (Chen et al., 2011; Conry et al., 2014; Kochanski et al., 2015; Mauree et al., 2018). All efforts considered, there is a paucity of robust and computationally efficient urban microclimate models that are capable of resolving spatial distribution of climate indicators such as wind, temperature, and humidity, while they are coupled to a nearby rural meteorological conditions as well as a building energy model. Numerous studies have used Computational Fluid Dynamics (CFD) to investigate the urban microclimate taking into account interactions between the atmosphere and the urban elements with full three-dimensional flow analysis (Saneinejad et al., 2012;

https://doi.org/10.5194/gmd-2019-176
Preprint. Discussion started: 27 August 2019

Geoscientific Model Development Discussions

Blocken, 2015; Nazarian and Kleissl, 2016; Aliabadi et al., 2017; Nazarian et al., 2018). Despite accurate predictions, CFD models are not computationally efficient, particularly for weather forecasting at larger scales and for a long period of time, and they usually do not represent many processes in the real atmosphere such as clouds and precipitation. As an alternative, UCMs require understanding of the interactions between the atmosphere and urban elements to parameterize various exchange processes of radiation, momentum, heat, and moisture within and just above the canopy, based on experimental data (Masson, 2000; Kusaka et al., 2001; Chin et al., 2005; Aliabadi et al., 2019), three-dimensional simulations, or simplified urban configurations (Martilli et al., 2002; Coceal and Belcher, 2004; Krayenhoff et al., 2014, 2015; Nazarian and Kleissl, 2016). These urban canopy models are more computationally efficient than CFD models. They are designed to provide more details on heat storage and radiation exchange, while they employ less detailed flow calculations.

Urban microclimate models must account for a few unique features of the urban environment. Urban obstacles such as trees and buildings contribute substantially to the changing of flow and turbulence patterns in cities (Kastner-Klein et al., 2004). Difficulties arise when the spatially inhomogeneous urban areas create highly three-dimensional wind patterns that result in the difficulty of parameterizations (Roth, 2000; Resler et al., 2017). For example, the surfaces of urban obstacles exert form and skin drag and consequently alter flow direction and produce eddies at different spatiotemporal scales. This can lead to the formation of shear layers at roof level with variable oscillation frequencies (Tseng et al., 2006; Masson et al., 2008; Zajic et al., 2011), all of such phenomena should be properly approximated in parameterizations.

Heat exchanges between the indoor and outdoor environments significantly influence the urban microclimate. Various studies have attempted to parametrize heat sources and sinks caused by buildings such as heat fluxes due to infiltration, exfiltration, ventilation, walls, roofs, roads, windows, and building energy systems (Kikegawa et al., 2003; Salamanca et al., 2010; Yaghoobian and Kleissl, 2012). Therefore, a Building Energy Model (BEM) is required to be properly integrated in an urban microclimate model to take account of the impact of building energy performance on the urban microclimate (Bueno et al., 2011, 2012b; Gros et al., 2014). This feedback interaction between the urban microclimate and indoor environment can significantly affect UHI and energy consumption of buildings (Adnot et al., 2003; Salamanca et al., 2014).

Urban vegetation can substantially reduce the adverse effects of UHI, particularly during heat waves, resulting in more thermal comfort (Grimmond et al., 1996; Akbari et al., 2001; Armson et al., 2012). Urban trees can potentially increase the overall albedo of a city, provide shade and shelter, and, therefore, change the energy balance of the individual buildings as well as the entire city (Akbari et al., 2001). A study of the local-scale surface energy balance revealed that the amount of energy dissipated due to the cooling effect of trees is not negligible and should be parameterized properly (Grimmond et al., 1996). In addition, the interaction between urban elements, most importantly trees and buildings, is evident in radiation trapping within the canyon and most importantly shading impact of trees (Krayenhoff et al., 2014; Redon et al., 2017; Broadbent et al., 2019). Buildings and trees obstruct the sky with implications in long and shortwave radiation fluxes downward and upward that may create unpredictable diurnal and seasonal changes in UHI (Futcher, 2008; Kleerekoper et al., 2012; Yang and Li, 2015). Also, it has been shown that not only trees but also the fractional vegetation coverage on urban surfaces can alter urban temperatures with implications in UHI (Armson et al., 2012). Trees, particularly those which are shorter than buildings, also exert drag and

https://doi.org/10.5194/gmd-2019-176
Preprint. Discussion started: 27 August 2019

Geoscientific Model Development Discussions

alter flow patterns within the canopy, however, this effect is not as significant as that drag induced by buildings (Krayenhoff et al., 2015). Such complex interactions must be accounted for in successful urban microclimate models.

1.1 Research Gaps

Numerous studies have focused on high fidelity urban microclimate models with high spatiotemporal flow resolution, capturing important features of the urban microclimate with acceptable accuracy (Gowardhan et al., 2011; Soulhac et al., 2011; Blocken, 2015; Nazarian et al., 2018). Despite the advances, however, high fidelity models capable of resolving three-dimensional flows, such as CFD or those extending to mesoscale weather forecasting, are not computationally efficient and they are complex to implement for operational applications. As a remedy, lower-dimensional flow urban microclimate models have been developed with many practical applications in city planning, architecture, and engineering consulting. For example, bulk flow (single-layer) models such as Urban Weather Generator (UWG) calculate the flow dynamics in one point, usually the centre of a hypothetical urban canyon, which is representative of all locations (Mills, 1997; Kusaka et al., 2001; Salamanca et al., 2010; Ryu et al., 2011; Bueno et al., 2012a, 2014). The Town Energy Balance (TEB) calculates energy balances for urban surfaces, which is forced by meteorological data and incoming solar radiation in the urban site with no connection to rural meteorological conditions (Masson et al., 2002). The Temperatures of Urban Facets - 3D (TUF-3D) model calculates urban surface temperatures with the main focus on three-dimensional radiation exchange, but it adopts bulk flow (single-layer) modelling without a connection to the surrounding rural area (Krayenhoff and Voogt, 2007). More recently TUF was coupled to an Indoor-Outdoor Building Energy Simulator (TUF-IOBES), but still this model adopted a bulk flow (single-layer) parameterization with no connection to the surrounding rural area (Yaghoobian and Kleissl, 2012). The multi-layer Building Effect Parametrization (BEP) model or its next generation BEP-Tree model include variable building heights, the vertical variation of climate variables and the effects of trees, but they are not linked to a building energy model (Martilli et al., 2002; Krayenhoff, 2014). More recently, the BEP model has been coupled to a Building Energy Model (BEP+BEM) but without a connection to the rural meteorological conditions. An overview of the literature reveals an apparent paucity of an independent urban microclimate model that accounts for some spatiotemporal variation of meteorological parameters in the urban environment and considers the effects of trees, building energy, radiation, and the connection to the rural meteorological conditions computationally efficiently and is operationally simple for practical applications.

1.2 Objectives

In this study, we present a new urban microclimate model, called the Vertical City Weather Generator (VCWG), which attempts to overcome some of the limitations mentioned in the previous section. It resolves vertical profiles (the direction that turbulent transport is significant) of climate parameters, such as temperature, wind, and humidity, in relation to urban design parameters. VCWG also includes a building energy model. It allows parametric investigation of design options on urban climate control at multiple heights, particularly if high density and high-rise urban design options are considered. This is a significant advantage over the bulk flow (single-layer) models such as UWG, which only consider one point for flow dynamics inside a hypothetical canyon (Masson, 2000; Kusaka et al., 2001; Dupont et al., 2004; Krayenhoff and Voogt, 2007; Lee and Park, 2008; Bueno

https://doi.org/10.5194/gmd-2019-176
Preprint. Discussion started: 27 August 2019

Geoscientific Model Development Discussions

et al., 2012a, 2014). The VCWG is designed to cycle through different atmospheric stability conditions that could be observed over the course of a day, but it is very computationally efficient with the capability to be run up to and beyond an entire year. The advantages of VCWG are as follows. 1) It does not need to be coupled to a mesoscale weather model because it functions standalone as a microclimate model. 2) Unlike many UCMs that are forced with climate variables above the urban roughness sublayer (e.g. TUF-3D), VCWG is forced with rural climate variables at 2m (temperature and humidity) and 10m (wind) elevation that are widely accessible and available around the world, making VCWG highly practical for urban design investigations at different climates. 3) VCWG provides urban climate information in one dimension, i.e. resolved vertically. This is advantageous over bulk flow (single-layer) models because vertical transport of momentum, heat, and atmospheric species is significantly important. 4) VCWG is coupled with the building energy model using feedback interaction.

VCWG is based on a predecessor bulk flow (single-layer) Urban Canopy Model (UCM), titled the Urban Weather Generator (UWG), which predicts the urban air temperature by assuming a relationship between urban and rural climates (Bueno et al., 2012a). UWG was used because it contains simple parameterizations of heat exchange processes between the key urban elements, particularly the building energy systems, and the atmosphere. It also imposes a low computational cost, enabling its usage to predict the urban microclimate on many spatial locations and over long periods of time (Bueno et al., 2014). UWG accounts for vegetation, but in rudimentary ways, only considering surface covered vegetation. So, it was extended in this study to include the effect of trees on the urban microclimate in more realistic ways with a predefined leaf area density profile. It is also extended to predict vertical profiles of temperature, specific humidity, wind in the urban environment based on models by Santiago and Martilli (2010), Krayenhoff et al. (2015), and Simón-Moral et al. (2017). The inclusion of trees in VCWG necessitated the implementation of new long and shortwave radiation models from Lee and Park (2008) and Redon et al. (2017), which calculate radiation heat heat fluxes in and out of a simplified infinite urban canyon. The remaining parameterizations within VCWG are extracted from other experimental field campaigns that particularly attempt to estimate the turbulent statistics (friction velocity and convective velocity scale), exchange velocity, and aerodynamic roughness lengths, in the rural and urban environments (Rotach et al., 2005; Balogun et al., 2010; Zajic et al., 2011; Roth et al., 2015; Aliabadi et al., 2019).

To evaluate the model, a microclimate field campaign in a representative urban area and a surrounding rural area was held in Guelph, Canada, during the Summer of 2018. Three components of wind velocity, temperature, relative humidity, and solar radiation were rigorously measured in this field campaign at different locations and under a comprehensive set of wind speeds, wind directions, and atmospheric stability conditions. To explore the model, the VCWG is set to run to investigate the effect of building dimensions, urban vegetations, and seasonal changes on the model outcome. The VCWG is also set to run for different climate zones for cities of Guelph, Buenos Aires, Tucson, Vancouver, Osaka, and Copenhagen.

1.3 Organization of the Article

The paper is structured as follows. Section 2 describes the methodology. In Sect. 2.1, all components of the VCWG and the way that they are integrated are presented. Firstly, the Rural Model (RM), used to determine the potential temperature profile and the horizontal pressure gradient in the rural area, is described. Then, details are discussed for the one-dimensional vertical diffusion model for the urban environment, the building energy model, and the radiation model, which are forced by the RM

https://doi.org/10.5194/gmd-2019-176
Preprint. Discussion started: 27 August 2019

Geoscientific Model Development Discussions

to predict the vertical profiles of meteorological quantities in the urban area. Sect. 2.2 describes the location and details of the field campaign, including meteorological instruments used. Section 3 provides the results and discussion. It starts with the evaluation of VCWG by comparing simulation results with those of the field measurements in Sect. 3.1. Then, results from other explorations including effects of building dimensions, foliage density, seasonal variation, different climate zones, and time series analysis on urban climate are presented in Sect. 3.2. Finally, Sect. 4 is devoted to conclusions and future work. Additional information about the equations used in the model and the details about the VCWG software are provided in the appendix.

2 Methodology

2.1 Vertical City Weather Generator (VCWG)

In this section, the Vertical City Weather Generator (VCWG) is introduced. Figure 1 shows the VCWG model schematic. VCWG consists of four integrated sub models including a Rural Model (RM) (Sect. 2.1.1) that forces meteorological boundary conditions on VCWG, a one-dimensional vertical diffusion model (Sect. 2.1.2) for calculation of the urban potential temperature, wind speed, turbulence kinetic energy, and specific humidity profiles, a Building Energy Model (BEM) (Sect. 2.1.3), and a radiation model with vegetation (Sect. 2.1.4). VCWG is based on the following predecessor models: a well-parameterized one-dimensional vertical diffusion model for urban microclimate variables known as the Building Effect Parametrization with Trees (BEP-Tree) model (Santiago and Martilli, 2010; Krayenhoff et al., 2014, 2015; Simón-Moral et al., 2017), an urban microclimate model with bulk flow (single-layer) and building energy parameterization known as the Urban Weather Generator (UWG) (Bueno et al., 2014), and a radiation model characterizing longwave (Lee and Park, 2008) and shortwave (Redon et al., 2017) radiation heat transfer in and out a two-dimensional urban canyon.

The sub models are integrated to predict vertical variation of urban microclimate parameters including potential temperature, wind speed, specific humidity, and turbulence kinetic energy as influenced by aerodynamic and thermal effect of urban elements including longwave and shortwave radiation exchanges, sensible heat fluxes released from urban elements, cooling effect of trees, and the induced drag by urban obstacles. Fig. 1 depicts the sub models in the VCWG and their relationship with each other. The Rural Model (RM) takes latitude, longitude, dry bulb temperature, relative humidity, dew point temperature, and pressure at $2\ \mathrm{m}$ elevation, wind speed and direction at $10\ \mathrm{m}$ elevation, horizontal infrared radiation intensity, global horizontal radiation, direct normal radiation, and diffuse horizontal radiation from an Energy Plus Weather (EPW) file [1]. For every time step, and forced with the set of weather data, the RM then computes a potential temperature profile, a constant specific humidity profile, and a horizontal pressure gradient, all of which are forced as boundary conditions to the one-dimensional vertical diffusion model in the urban area. The potential temperature and specific humidity are forced as fixed values on top of the domain for the urban vertical diffusion model in the temperature and specific humidity equations, respectively. The horizontal pressure gradient is forced as a source term for the urban vertical diffusion model in the momentum equation. While forced

[1] https://energyplus.net/weather

https://doi.org/10.5194/gmd-2019-176
Preprint. Discussion started: 27 August 2019

Geoscientific Model Development Discussions
Open Access
EGU

by the RM, the urban one-dimensional vertical diffusion model is also coupled with a building energy model and the two-dimensional radiation model. The three models have feedback interaction and converge to a solution (temperature and wind speed) iteratively. The urban one-dimensional vertical diffusion model calculates the flow quantities at the centre of control volumes, which are generated by splitting the urban computational domain into multiple layers within an above the urban canyon (see Fig. 4). The urban domain extends to five times building height that conservatively includes the entire roughness sublayer within the atmospheric boundary layer (Santiago and Martilli, 2010; Aliabadi et al., 2017). The feedback interaction coupling scheme among the building energy model, radiation model, and the urban one-dimensional vertical diffusion model is designed to update the boundary conditions, surfaces temperatures, and the source/sink terms in the transport equations. For each time step, the iterative calculation for all the sub models continues until the convergence criterion of temperature and wind speed in the canyon are fulfilled. More details about the sub models are provided in the subsequent sections and the appendix.

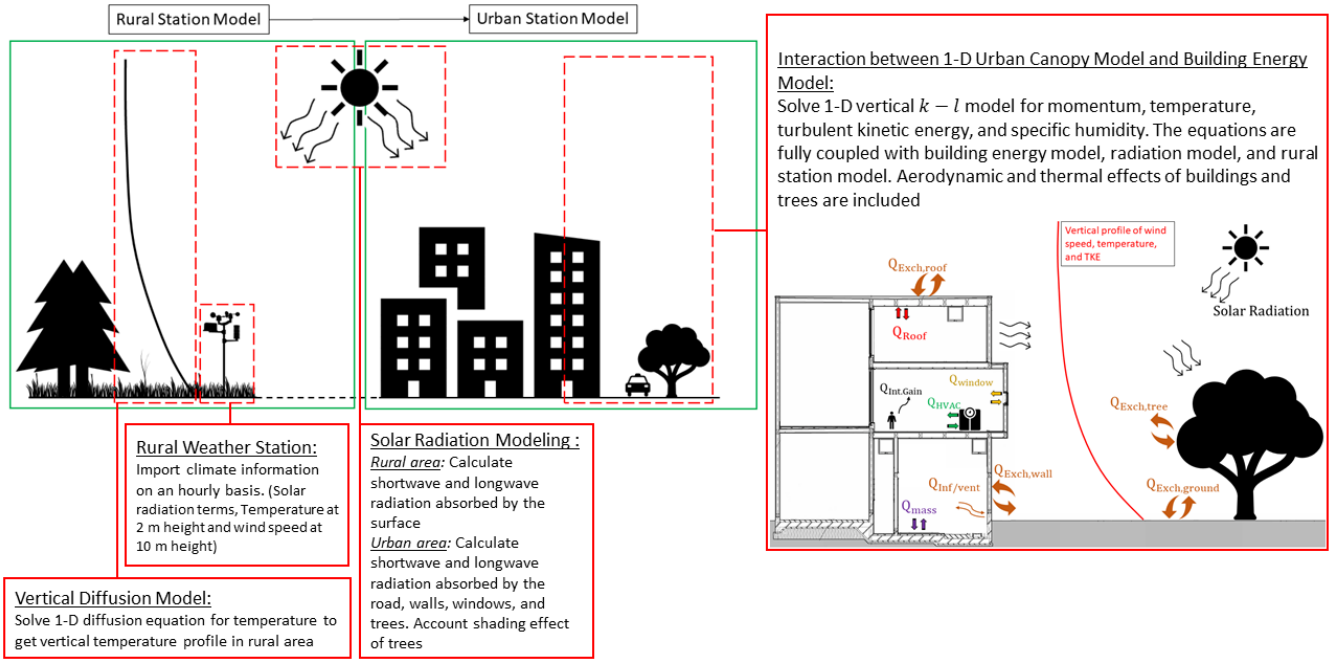

Figure 1. The schematic of Vertical City Weather Generator (VCWG).

2.1.1 Rural Model

Throughout the VCWG development, Reynolds averaging is used for meteorological variables so the instantaneous variable is the sum of the time-averaged part plus the turbulent fluctuating part, i.e. $X=\overline{X}+x$, where X represents the instantaneous variable of interest, $\overline{X}$ is the time-averaged variable, and x is the fluctuating part of the variable. In the rural model (see Fig. 1), a Vertical Diffusion Model (VDM) calculates the vertical profile of potential temperature in the rural site using meteorological

https://doi.org/10.5194/gmd-2019-176
Preprint. Discussion started: 27 August 2019

Geoscientific Model Development Discussions

information measured at the weather station. The atmospheric variation of potential temperature in the vertical direction is assumed to be quasi-steady. At every time step of the model, the temperature at the lowest level is forced by rural measurements at 2 m, i.e. from a weather file, then the VDM predicts the vertical structure of potential temperature using the forced temperature and other parameters such as a source/sink term, diffusion coefficient, and mixing length. It is also assumed that the rural area is horizontally homogeneous and very flat. The combination of input parameters are sourced from an Energy Plus Weather (EPW) database[2]. The mean potential temperature is parameterized using the gradient-diffusion hypothesis,

$$0 = \frac{\partial}{\partial z}(-\frac{K_m}{Pr_t}\frac{\partial \overline{\Theta}_{rur}}{\partial z}) + \gamma, \tag{1}$$

where $\overline{\Theta}_{\mathrm{rur}}$ is potential temperature in the rural site, $\mathrm{K_m}$ is turbulent diffusivity for momentum, $\mathrm{Pr_t}$ is turbulent Prandtl number, γ is heat source/sink term, and z is the vertical coordinate. It has been suggested that turbulent Prandtl number $\mathrm{Pr_t}$ varies between 0.25 to 1.5 depending on atmospheric stability and scale of analysis and decreases under more unstable conditions (Raupach et al., 1996; Grachev et al., 2007; Aliabadi et al., 2016b; Li, 2018). In this study, for simplicity, $\mathrm{Pr_t}$ is set to be 0.8, but it can be changed as the input of the model.

Two approaches have been suggested to formulate $\mathrm{K_m}$, based on uniform turbulent viscosity and the mixing-length model (Pope, 2000). The former considers a constant turbulent viscosity that is suitable only for simple shear flows. In the mixing length model, which is more applicable in boundary layer flows, $\mathrm{K_m}$ is proportional to the mixing-length (ℓ) and the gradient of mean horizontal wind speed ($\overline{\mathrm{S}}_{\mathrm{rur}}$)

$$K_m = \ell^2 \frac{\partial \overline{S}_{rur}}{\partial z}. \tag{2}$$

A log-law is assumed for wind profile given an aerodynamic roughness length $\mathrm{z_0}$ and wind measurement at 10 m. From the corresponding log-law the vertical gradient of wind speed is calculated analytically by simple differentiation of the log-law and then used to determine momentum diffusivity. Numerous studies have attempted to parameterize mixing-length based on the well-known Obukhov length (Peña et al., 2010; Sun, 2011; Keck et al., 2014; Sun et al., 2016), which is the ratio of shearing to buoyancy effects representing the atmospheric stability condition. It has been shown that such models break down in neutral or weakly stable conditions, when the vertical turbulent heat flux approaches zero (Grachev et al., 2013; Aliabadi et al., 2016a; Optis et al., 2016; Sun et al., 2016). In this study, the thermal stability condition is roughly approximated based on the available incoming solar radiation in the way that presence or absence of incoming solar radiation on the surface indicate unstable and stable conditions, respectively. The mixing length can be obtained by (Gryning et al., 2007)

$$\frac{1}{\ell} = \frac{1}{C_{crur}}(\frac{1}{\kappa z} + \frac{1}{C_* u_*}), \tag{3}$$

where the first term on the right-hand side indicates a linear relationship with height near the surface, while the second term restricts the value of length scale in the upper part of the atmospheric surface layer asymptotically. $\mathrm{C_{crur}}$ is a scaling correction factor, which is optimized to 1 during unstable conditions and 1.5 during stable conditions, $\mathrm{C_*}$ is a model constant optimized

[2]https://energyplus.net/weather

https://doi.org/10.5194/gmd-2019-176
Preprint. Discussion started: 27 August 2019

Geoscientific Model Development Discussions

to be 1, and κ=0.4 is von Kármán constant. Friction velocity u_* was parameterized based on field data from a previous microclimate field campaign in rural and urban areas located in Guelph, Canada (Aliabadi et al., 2019)

$$u_* = 0.07\overline{S}_{rur} + 0.12. \tag{4}$$

It is suggested that thermal exchange processes within the atmospheric surface layer are tightly coupled to heat transfer with the earth surface (Stull, 1988). When the surface is warmer than air, upward heat flux released into the atmosphere creates a thermally unstable condition. On the other hand, downward heat flux, mostly observed over night when the surface is cooling, creates a thermally stable condition. Sensible heat fluxes are required to estimate γ. Meteorological information obtained from the weather station including direct and diffuse solar radiation, temperature at the height of 2 m, and wind speed at the height of 10 m are used to calculate the net heat flux at the surface

$$Q_{net,rur} = \underbrace{Q_{Hveg,rur} + h_{conv}(T_{0,rur} - T_{air,rur}) + Q_{rad,rur}}_{\text{sensible heat flux}}, \tag{5}$$

where $\mathrm{Q_{net,rur}}$ is the net heat flux (positive upward from the surface into the atmosphere at the rural site), $\mathrm{Q_{Hveg,rur}}$ is the sensible heat flux from biogenic activity of vegetation, $\mathrm{h_{conv}}$ is the convection heat transfer coefficient at the surface, $\mathrm{T_{0,rur}}$ is the rural surface temperature calculated by the rural model, $\mathrm{T_{air,rur}}$ is the air temperature at the height of 2 m, and $\mathrm{Q_{rad,rur}}$ is the longwave and shortwave radiation absorbed by rural surface (for more details see Appendix A). Therefore, the heat sink/source term in Eq. 1 can be parameterized as

$$\gamma = C_\gamma \left(\frac{Q_{net,rur}}{\rho C_p}\right) \frac{1}{H_{bl}}, \tag{6}$$

where ρ is air density near the rural surface, $\mathrm{C_p}$ is air specific heat capacity, $\mathrm{C_\gamma}$ is a scaling factor for heat sink/source term equal to 10, and $\mathrm{H_{bl}}$=2000 m is the diurnally-averaged boundary-layer height. Numerous studies have focused on parameterization of convection heat transfer coefficient reviewed by Palyvos (2008). In this study, the following boundary-layer type correlation between $\mathrm{h_{conv}}$ and mean wind speed ($\mathrm{\overline{S}_{rur}}$) is used

$$h_{conv} = 3.7\overline{S}_{rur} + 5.8. \tag{7}$$

The rural model also outputs a horizontal pressure gradient based on friction velocity calculation that is later used as a source term for the urban one-dimensional vertical diffusion momentum equation. The pressure gradient is parameterized as $\rho \mathrm{u_*^2/H_{avg}}$. This choice does not necessitate a need for solving a vertical diffusion equation for momentum in the rural area.

Another assumption made in the rural model is that the specific humidity is constant in the vertical direction, i.e. invariant with height, for the lowest range of the atmospheric surface layer. This assumption is valid so long as the water vapour pressure is less than the saturation water vapour pressure for a given altitude. This condition must be checked to confirm the adequacy of this assumption. The specific humidity can be calculated from the ratio of water vapour density to the air density, which can be simplified using ideal gas law Q=0.622$\mathrm{P_v/P_a}$, where $\mathrm{P_v}$ is water vapor pressure and $\mathrm{P_a}$ is the air pressure. We can calculate the saturation pressure ($\mathrm{P_{sat}}$) using the Clausius-Clapeyron equation

$$P_{sat} = 6.1094 \exp\left(\frac{17.625 T_{rur}}{T_{rur} + 243.04}\right). \tag{8}$$

https://doi.org/10.5194/gmd-2019-176
Preprint. Discussion started: 27 August 2019

Geoscientific Model Development Discussions

A density profile is required to convert the real temperature profile in the rural area ($\mathrm{T_{rur}}$) to potential temperature profile and vice versa, which is used in the Eq. 1. Using a reference density (ρ_0), reference temperature ($\mathrm{T_0}$), and reference pressure ($\mathrm{P_0}$) at the surface level from the weather station at 2 m elevation, and considering a lapse rate of $-0.000133\ \mathrm{kg\ m^{-3}\ m^{-1}}$ for density within the surface layer, the density profile can be simplistically parameterized by

$$\rho = \rho_0 - 0.000133(z - z_0). \tag{9}$$

After checking that the condition is met for constancy of specific humidity with height, the specific humidity calculated by the rural model can be applied as a fixed value boundary condition at the top of the domain in the urban one-dimensional vertical diffusion model in the specific humidity transport equation.

2.1.2 Urban Vertical Diffusion Model

Numerous studies have attempted to parameterize the interaction between urban elements and the atmosphere in terms of dynamical and thermal effects, from very simple models based on Monin-Obukhov similarity theory (Stull, 1988), to the bulk flow (single-layer) parameterizations (Krayenhoff and Voogt, 2007; Masson, 2000; Kusaka et al., 2001; Bueno et al., 2014), to multi-layer models (Hamdi and Masson, 2008; Santiago and Martilli, 2010; Krayenhoff et al., 2015) with different levels of complexity. The multi-layer models usually treat aerodynamic and thermal effects of urban elements as sink or source terms in momentum, heat, specific humidity, and turbulence kinetic energy equations. Parameterization of the exchange processes between the urban elements and the atmosphere can be accomplished using either experimental data or CFD simulations (Martilli et al., 2002; Dupont et al., 2004; Kondo et al., 2005; Kono et al., 2010; Lundquist et al., 2010; Santiago and Martilli, 2010; Krayenhoff et al., 2015; Aliabadi et al., 2019). CFD-based parameterizations proposed by Martilli and Santiago (2007), Santiago and Martilli (2010), and Krayenhoff et al. (2015) use results from Reynolds-Averaged Navier-Stokes (RANS) simulations including effects of trees and buildings. These parameterizations consider the CFD results at different elevations after being temporally and horizontally averaged.

For the one-dimensional vertical diffusion model, any variable such as cross- and along-canyon wind velocities (U and V, respectively), potential temperature (Θ), and specific humidity (Q) is presented using Reynolds averaging. The one-dimensional time-averaged momentum equations in the cross- and along-canyon components, which are originally developed by Santiago and Martilli (2010), can be shown as

$$\frac{\partial \overline{U}}{\partial t} = \underbrace{-\frac{\partial \overline{uw}}{\partial z}}_{I} \underbrace{-\frac{1}{\rho}\frac{\partial \overline{P}}{\partial x}}_{II} \underbrace{-D_x}_{III}, \tag{10}$$

$$\frac{\partial \overline{V}}{\partial t} = \underbrace{-\frac{\partial \overline{vw}}{\partial z}}_{I} \underbrace{-\frac{1}{\rho}\frac{\partial \overline{P}}{\partial y}}_{II} \underbrace{-D_y}_{III}, \tag{11}$$

where $\overline{\mathrm{P}}$ is time-averaged pressure. The terms on the right hand side of Eqs. 10 and 11 are the vertical gradient of turbulent flux of momentum (I), acceleration due to the large-scale pressure gradient (II), and the sum of pressure, building form,

https://doi.org/10.5194/gmd-2019-176
Preprint. Discussion started: 27 August 2019

Geoscientific Model Development Discussions

building skin, and vegetation drag terms (III). The parameterization of the latter term is detailed in Appendix A based on studies by Santiago and Martilli (2010) and Krayenhoff et al. (2015) and is not reported here for brevity. K-theory was used to parameterize the vertical momentum fluxes, i.e. $\partial\overline{uw}/\partial z = -K_m\partial\overline{U}/\partial z$ and $\partial\overline{vw}/\partial z = -K_m\partial\overline{V}/\partial z$ (the same approach will be used in energy and humidity equations), where the diffusion coefficient is calculated using a $\mathrm{k}-\ell$ model

$$K_m = C_k \ell_k k^{1/2}, \tag{12}$$

where $\mathrm{C_k}$ is a constant and ℓ_k is a length scale optimized using CFD. $\mathrm{C_k}$ can be obtained based on the bulk Richardson number $\mathrm{Ri_b}=\mathrm{gH_{avg}}\Delta\overline{\Theta}/(\Delta\overline{\mathrm{S}}^2\overline{\Theta}_\mathrm{avg})$, where g is gravitational acceleration, $\mathrm{H_{avg}}$ is average building height, $\Delta\overline{\Theta}$ and $\Delta\overline{\mathrm{S}}$ are the variation of temperature and horizontal wind speed over vertical distance $\mathrm{H_{avg}}$ (i.e. roof level minus street level), and $\overline{\Theta}_\mathrm{avg}$ is the mean temperature in the canyon. After performing an optimization procedure the best value of $\mathrm{C_k}$ was determined depending on a critical bulk Richardson number, which is set to 0.01, $\mathrm{C_k}$=4 for unstable condition ($\mathrm{Ri_b} > 0.01$) and $\mathrm{C_k}$=2 for stable condition ($\mathrm{Ri_b} < 0.01$). More details on $\mathrm{C_k}$ and ℓ_k are provided in Krayenhoff (2014). The turbulence kinetic energy k can be calculated using a prognostic equation (Stull, 1988)

$$\frac{\partial k}{\partial t} = \underbrace{K_m\left[\left(\frac{\partial\overline{U}}{\partial z}\right)^2+\left(\frac{\partial\overline{V}}{\partial z}\right)^2\right]}_{I} + \underbrace{\frac{\partial}{\partial z}\left(\frac{K_m}{\sigma_k}\frac{\partial k}{\partial z}\right)}_{II} - \underbrace{\frac{g}{\Theta_0}\frac{K_m}{Pr_t}\frac{\partial\overline{\Theta}}{\partial z}}_{III} + \underbrace{S_{wake}}_{IV} - \underbrace{\varepsilon}_{V}, \tag{13}$$

where g is acceleration due to gravity and Θ_0 is a reference potential temperature. The terms on the right hand side of Eq. 13 are shear production (I), turbulent transport of kinetic energy parameterized based on K-theory (II), buoyant production/dissipation (III), wake production by urban obstacles (IV), and dissipation (V). Parameterization of the last two terms is presented in more details in Appendix A and Krayenhoff (2014) and not reported here for brevity. σ_k is turbulent Prandtl number for kinetic energy, which is generally suggested to be σ_k=1 (Pope, 2000).

To calculate vertical profile of potential temperature in the urban area, the transport equation can be derived as

$$\frac{\partial\overline{\Theta}}{\partial t} = \underbrace{\frac{\partial}{\partial z}\left(\frac{K_m}{Pr_t}\frac{\partial\overline{\Theta}}{\partial z}\right)}_{I} + \underbrace{S_{\Theta R}+S_{\Theta G}+S_{\Theta W}+S_{\Theta V}+S_{\Theta A}+S_{\Theta waste}}_{II}, \tag{14}$$

where the first term on the right hand side is turbulent transport of heat (I) and the heat sink/source terms (II) correspond to sensible heat exchanges with roof ($\mathrm{S_{\Theta R}}$), ground ($\mathrm{S_{\Theta G}}$), wall ($\mathrm{S_{\Theta W}}$), urban vegetation $\mathrm{S_{\Theta V}}$, and radiative divergence $\mathrm{S_{\Theta A}}$ detailed in appendix A and by Krayenhoff et al. (2014) and not reported here for brevity (see Fig. 1). Contribution of the waste heat emissions from building heating ventilation and air conditioning (HVAC) system $\mathrm{S_{\Theta waste}}$ is parameterized by

$$S_{\Theta waste} = F_{st}\frac{1}{\rho C_p \Delta z}Q_{HVAC}, \tag{15}$$

where $\mathrm{Q_{HVAC}}$ is total sensible waste heat released into the urban atmosphere, $\mathrm{F_{st}}$ is the fraction of waste heat released at street level, while the remainder fraction $1-\mathrm{F_{st}}$ is released at roof level, and Δz is grid discretization in the vertical direction.

https://doi.org/10.5194/gmd-2019-176
Preprint. Discussion started: 27 August 2019

Geoscientific Model Development Discussions

Depending on the type of building, waste heat emissions can be released partially at street level and the rest at roof level, which can be adjusted by changing F_{st} from 0 to 1. In this study, it is set to 0.1.

To complete the urban one-dimensional vertical diffusion model (see Fig. 1), the transport equation for specific humidity is

$$\frac{\partial \overline{Q}}{\partial t} = \underbrace{\frac{\partial}{\partial z}\left(\frac{K_m}{Sc_t}\frac{\partial \overline{Q}}{\partial z}\right)}_{I} + \underbrace{S_{QV}}_{II}, \tag{16}$$

where $\overline{Q}$ is time-averaged specific humidity. The turbulent transport of specific humidity (I) is parameterized based on K-theory, Sc_t is turbulent Schmidt number set to 1 in this study, and source term S_{QV} (II) is caused by latent heat from vegetation detailed in appendix A and by Krayenhoff (2014) but not reported here for brevity.

2.1.3 Building Energy Model

Building energy consumption due to HVAC systems and the associated interaction with the urban atmosphere can alter the urban microclimate. It has been reported that such interaction can change UHI depending on the region and climate of interest (De Munck et al., 2013; Schoetter et al., 2017). In this study, the balance equation for convection, conduction, and radiation heat fluxes is applied to all building elements (wall, roof, floor, windows, and internal mass) to calculate the indoor air temperature. Then, a sensible heat balance equation, between convective heat fluxes released from indoor surfaces and internal heat gain and sensible heat fluxes from HVAC system and infiltration, is solved to obtain the time evolution of indoor temperature as

$$\forbar{V}\rho C_p \frac{dT_{in}}{dt} = \Sigma Q_{cv,i} + Q_{gain} + Q_{inf/exf} + Q_{sys}, \tag{17}$$

where $\forbar{V}$ is indoor volume, T_{in} is indoor air temperature, $Q_{cv,i}$ is heat conduction from the building elements, Q_{gain} is internal heat gain, $Q_{inf/exf}$ is heat associated with infiltration or exfiltration, and Q_{sys} is heat released from the air conditioning system. More details on parameterization of the terms in Eq. 17 can be found in appendix A and Bueno et al. (2012b) but are not reported here for brevity.

The same balance equation can be derived for latent heat to determine the time evolution of the indoor air specific humidity Q_{in}

$$\forbar{V}\rho L_v \frac{dQ_{in}}{dt} = Q_{gain} + Q_{inf} + Q_{sys}, \tag{18}$$

which is composed of latent heat gain Q_{gain}, infiltration latent heat Q_{inf}, and latent heat from the air conditioning system Q_{sys}. The terms on the right hand side of Eq. 18 are parameterized in Bueno et al. (2012b) but are not detailed here for brevity.

2.1.4 Radiation Model with Vegetation

Urban trees provide shade to buildings and ground and reduce the amount of shortwave radiation within the urban canyon by reflection and transmission. It has been shown that a fraction of shortwave and longwave radiation is reflected or transmitted by leaves, variable depending on species of trees (Kong et al., 2017). As a result, trees can reduce surface temperatures significantly

https://doi.org/10.5194/gmd-2019-176
Preprint. Discussion started: 27 August 2019

and consequently improve thermal comfort during the Summer. On the other hand, trees can induce drag and lower the wind speed within the urban area that can potentially contribute to reduced ventilation rates within the urban canyon (Krayenhoff et al., 2015). Therefore, interactions between building and vegetation and their impact on the urban environments should be understood and modelled in detail. Only few studies have included such interactions in the urban microclimate models (Lee and Park, 2008; Krayenhoff et al., 2015; Redon et al., 2017).

In VCWG, there are two types of vegetation: surface covered vegetation and trees. Surface covered vegetation is specified by surface fraction covered by vegetation. Tree vegetation is specified by three parameters: Leaf Area Index (LAI), Leaf Area Density (LAD) profile, and trunk height. Both types of vegetation are specified with the same albedo. The VCWG user can change these input parameters for different vegetation structures. The parameterization of shortwave radiation accounts for the incoming direct and diffuse components of solar radiation, and it is used in this study to account for the shading effects of trees on vertical and horizontal urban surfaces as well as the shading effect of buildings on trees. The total amount of shortwave radiation absorbed by each urban element is calculated by adding the before-reflection absorption of shortwave radiation to the sum of multiple infinite reflections within the canyon (Redon et al., 2017). Parameterization of the longwave radiation received and emitted by the urban elements is based on two assumptions that the surfaces are Lambertian and that only one reflection is allowed (Lee and Park, 2008). Both shortwave and longwave radiation models are coupled to the vertical diffusion and the building energy models using feedback interaction. Detailed formulations are not provided here for brevity, but the reader is referred to the appendix A and original studies by Redon et al. (2017) and Lee and Park (2008).

2.2 Experimental Field Campaign

2.2.1 Logistics

To evaluate results from VCWG, comprehensive microclimate field measurements were conducted from 15 July 2018 to 5 September 2018, in Guelph, Canada, which is detailed below. Guelph is located in southwestern Ontario, Canada, with cold Winters and humid Summers. The urban microclimate field measurements were conducted in the Reek Walk, a typical quasi two-dimensional urban canyon, located at the University of Guelph (43.5323°N and 80.2253°W). The rural microclimate field measurements were conducted in the Guelph Turfgrass Institute, a research green space area located at 43.5473°N and 80.2149°W, about 2 km northeast of the Reek Walk. The average building height for the urban area is H_{avg}=20 m, and the plan area density is λ_p=0.55. The road, Reek Walk, where meteorological instruments are installed, is covered by grass and asphalt in equal fractions. As shown in Fig. 2, urban trees are distributed across the neighbourhood.

The urban canyon axis is oriented in the northwest-southeast direction and x and y directions are set to be cross- and the along-canyon, respectively (see Fig. 3). The frontal area density λ_f varies from 0.31 to 0.51 when the approaching wind direction changes from along- to cross-canyon, respectively. Figure 3 shows that the predominant wind directions were from west and southwest, roughly perpendicular to the canyon axis, for the field campaign duration. Based on studies aimed to characterize the wind flow pattern within a built-up area (Zajic et al., 2011; Grimmond and Oke, 1999), the observed flow

https://doi.org/10.5194/gmd-2019-176
Preprint. Discussion started: 27 August 2019

Geoscientific Model Development Discussions
Open Access
EGU

configuration alternates between skimming flow and wake interface regimes. However, the flow within the urban site is more complicated than the simple regimes and the associated parametrizations.

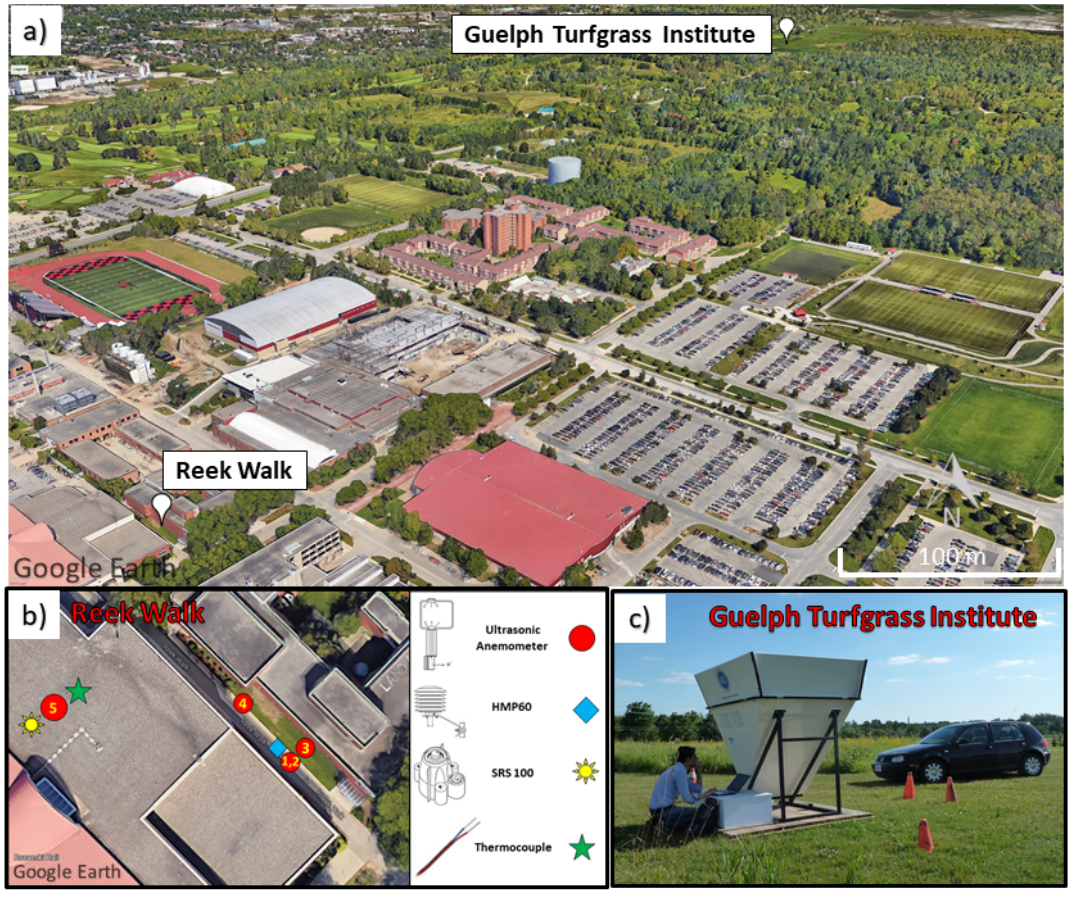

Figure 2. (a) Top view of the rural (Guelph Turfgrass Institute) and the urban (Reek Walk, University of Guelph) weather stations; (b) location of meteorological instruments in the urban site; (c) rural weather station and the Doppler miniSoDAR instrument operated in the rural area; images were obtained from © Google Earth.

2.2.2 Instruments

In the rural site, wind speed, wind direction (at 10 m), relative humidity, and temperature (at 2 m) are collected on an hourly basis by the Guelph Turfgrass Institute meteorological station, which bears World Meteorological Organization (WMO) identifier 71833. As shown in Fig. 2c, A Doppler mini SOnic Detection And Ranging (miniSODAR) instrument from Atmospheric Systems Corporation (ASC)[3] was also operated to measure wind speed and wind direction from 30 m to 200 m altitude at

[3]http://www.minisodar.com/sodar/

https://doi.org/10.5194/gmd-2019-176
Preprint. Discussion started: 27 August 2019

Geoscientific Model Development Discussions

10-m vertical resolution, which output averaged data every 30 minutes. The miniSODAR data is not reported for brevity, but it was used to evaluate the reported WMO meteorological measurements.

In the urban site, meteorological information was collected within and above the canyon using five 81000 R. M. Young ultrasonic anemometers from Young U.S.A.[4] distributed horizontally and vertically. The accuracy and resolution of measurements for wind speed were $\pm 1\%$ and 0.01 $\mathrm{m\,s^{-1}}$, respectively, and for temperature were ± 2 K and 0.01 K, respectively. Four anemometers were deployed within the canyon, two were placed on a pole at heights of 2.4 m and 5.5 m from the ground and the other two anemometers were located 4 m and 30 m away from the pole in the cross- and along-canyon directions, respectively. The fifth anemometer was deployed on a tripod on the roof at 2.5 m height from roof level (see Fig. 2b). Three of these anemometers located at different elevations were used for comparison to VCWG model results. It has been suggested that the sampling frequency should be at least 10 Hz to measure turbulence (Balogun et al., 2010; Giometto et al., 2016). The anemometers were adjusted to sample three components of wind speed and air temperature at a frequency of 20 Hz using Campbell Scientific[5] CR6 data loggers. A Pace SRS-100 solar radiation sensor from Pace Scientific[6] was placed at the roof to measure solar irradiance every minute with a resolution of 1 $\mathrm{Wm^{-2}}$. Type E thermocouples from Omega[7] were also used near the surfaces at street and roof levels to measure temperature every minute. Data from the thermocouple sensors are not reported for brevity. As shown in Fig. 2b, a Campbell Scientific HMP60 sensor was deployed at the street level, which measured minute-averaged relative humidity with an accuracy of $\pm 3\%$ and temperature with an accuracy of ± 0.6K.

Wind tunnel tests were conducted to calibrate the wind speeds measured by the ultrasonic anemometers against a reference pitot tube (No figures are shown for this calibration). The HMP60 sensor was used as the reference measurement to calibrate all other temperatures and relative humidities measured, including those of the WMO station.

3 Results and Discussion

In this section, the VCWG model results are compared to the microclimate field measurements. We also explored the capability of the model to predict urban climate for various urban configurations and in different climate conditions. The simplified urban neighbourhood is depicted in Fig. 4. In VCWG, buildings with uniformly-distributed height, equal width, and equal spacing from one another, represent the urban area. The computational domain height is five times the average building height, which makes it suitable for microclimate analysis (Santiago and Martilli, 2010; Aliabadi et al., 2017). A uniform Cartesian grid with 2 m vertical resolution is used, where buildings are removed from control volumes (see Fig. 4). The flow is assumed to be pressure-driven with the pressure gradient of $\rho \mathrm{u}_*^2/\mathrm{H}_{\mathrm{avg}}$, which is decomposed into the x and y directions based on the wind angle. In this equation, the adjustment for wind angle is made based on canyon orientation and the incoming wind angle at the top of the domain. The boundary condition for potential temperature and humidity equations (Eqs. 14 and 16) are determined from the rural model (see Fig. 1). Thus, the VCWG is aimed to calculate momentum and energy exchanges for the centre of

[4] http://youngusa.com/
[5] https://www.campbellsci.ca
[6] https://www.pace-sci.com
[7] https://www.omega.ca

https://doi.org/10.5194/gmd-2019-176
Preprint. Discussion started: 27 August 2019

Geoscientific Model Development Discussions

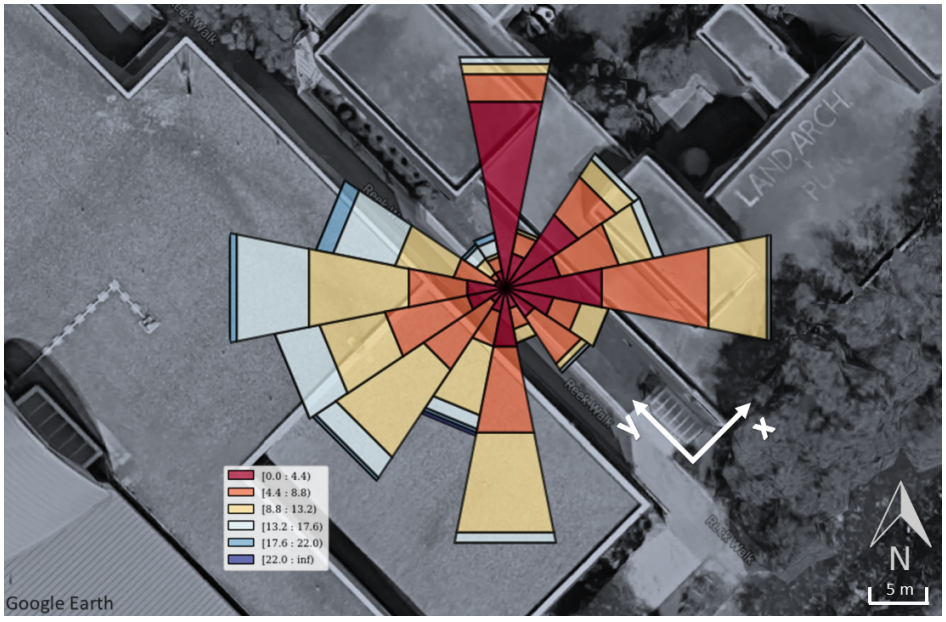

Figure 3. Wind rose plot above the urban site (Reek Walk, University of Guelph) between 15 July 2018 and 5 September 2018; image was obtained from © Google Earth.

each cell in the vertical direction based on the boundary conditions obtained from the rural model, the building energy model, and the radiation model.

Fig. 5 shows the time series of P_{sat} and P_v on the top of the domain over the course of a day in the rural area. Vapour pressure is always less than saturation pressure. However, vapour pressure tends closer to the saturation pressure under strongly stable condition from 0000 Local Solar Time (LST) to 0600 LST. Assuming constant specific humidity up to the height of five times of average building height in the rural area does not violate the requirement for constancy of the water vapour pressure with height. Note, however, that this assumption does not apply to high altitudes where condensation may occur due to water vapour pressure exceeding saturation vapour pressure.

3.1 Model-Observation Comparison

Temperature observations from Aircraft Meteorological Data Reports (AMDAR) in the Kansas City International airport (MCI) for 15 August 2018 was used to evaluate the results of the VCWG in the rural area. The commercial aircraft, mostly in North America, measure planetary boundary layer profiles of meteorological variables during climb and descent. The data are archived by National Oceanic and Atmospheric Administration (NOAA) and are freely available, which is accessed via the Meteorological Assimilation Data Ingest System (MADIS) portal [8]. These measurements are widely used to evaluate weather

[8] https://amdar.noaa.gov/

https://doi.org/10.5194/gmd-2019-176
Preprint. Discussion started: 27 August 2019

Geoscientific Model Development Discussions

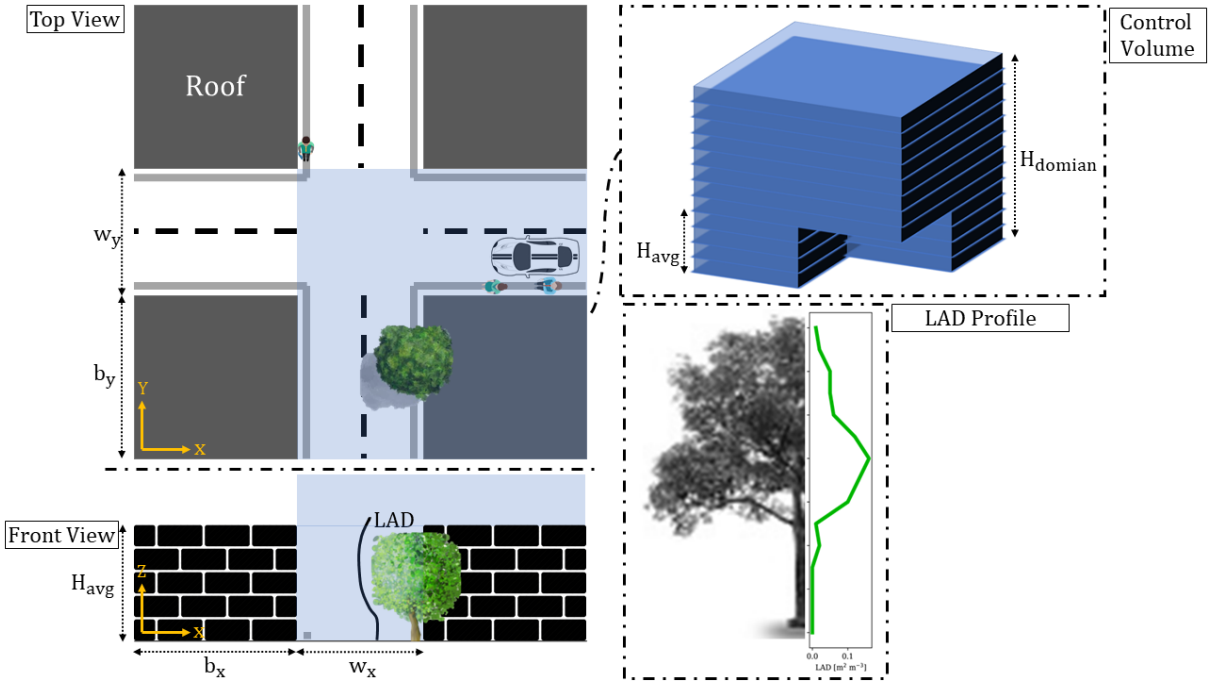

Figure 4. Simplified urban area used in VCWG and corresponding layers of control volumes within and above the canyon. The height of the domain is five times of the average building height.

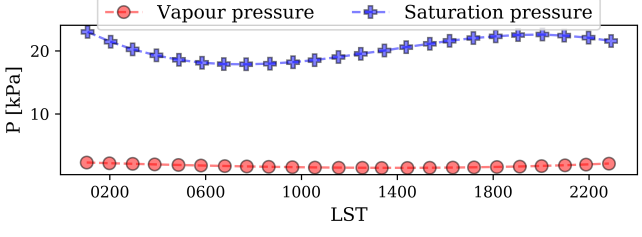

Figure 5. Diurnal variation of water vapour pressure and saturation vapour pressure on the top of the domain for the rural model.

https://doi.org/10.5194/gmd-2019-176
Preprint. Discussion started: 27 August 2019

Geoscientific Model Development Discussions
Open Access
EGU

forecasting models and to understand climate under different conditions (Moninger et al., 2010; Zhang et al., 2019). AMDAR data report pressure altitude as the vertical position of the aircraft, which can be converted to pressure using the equation proposed by WMO (2003)

$$P = 1013.25\left(1 - \frac{0.3048 z_p}{145366.45}\right)^{5.2553}, \tag{19}$$

where P is pressure in hPa and $\mathrm{z_p}$ is pressure altitude in ft. Then, the hypsometric equation can be used to determine the actual vertical position of the aircraft (Stull, 2016). Figure 6 shows the comparison between aircraft measured data and the rural model prediction of potential temperature profiles. The rural model is in reasonable agreement with the measured data and it can capture the atmospheric stability conditions and diurnal variation in potential temperature over a course of the day.

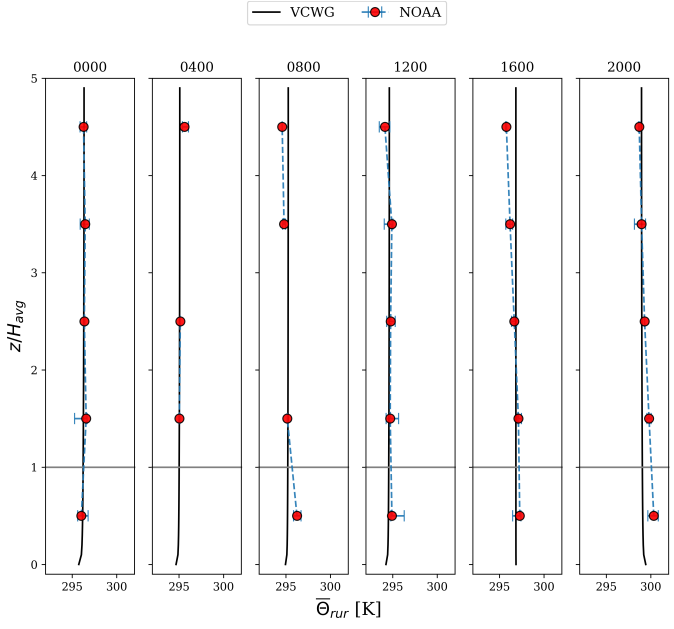

Figure 6. Comparison between the AMDAR data and the VCWG prediction of potential temperature profiles in the rural site.

The results of the VCWG are now compared to the measured data in the microclimate field campaign. The actual weather data in the rural area including wind speed and wind direction at $10\ \mathrm{m}$ height, temperature and relative humidity at $2\ \mathrm{m}$ height, atmospheric pressure, and terms describing radiative components are used from the WMO and the field campaign datasets. The input parameters representing the urban area are listed in Table 1. The simulations were run for two days starting from 19 August 2018 with the first 24 hours treated as model spin-up period. For such analysis, the run time is approximately 15 minutes, however it can vary slightly depending on the grid size.

Vertical profiles of potential temperature, mean horizontal wind speed, and specific humidity at street level are compared with the measurements at three heights in the urban area (see Figs. 7-9). Additionally, normalized mean square error (NMSE)

https://doi.org/10.5194/gmd-2019-176
Preprint. Discussion started: 27 August 2019

Geoscientific Model Development Discussions

Table 1. List of input parameters used to evaluate the VCWG (The LAD profile used for validation is shown in Fig. 4).

Parameter	Symbol	Value
Latitude °N	lat	43.53
Longitude °W	lon	80.22
Season	-	Summer
Plan area density	λ_{p}	0.44
Frontal area density	λ_{f}	0.55
Average buildings height [m]	$\mathrm{H_{avg}}$	20
Average of leaf area density profile [$\mathrm{m^2 m^{-3}}$]	LAD	0.048
Building Type	-	Office
Urban Albedos (roof, ground, wall, vegetation)	$\alpha_{\mathrm{R}}, \alpha_{\mathrm{G}}, \alpha_{\mathrm{W}}, \alpha_{\mathrm{V}}$	0.13, 0.1, 0.2, 0.25
Urban Emissivities (roof, ground, wall, vegetation)	$\varepsilon_{\mathrm{R}}, \varepsilon_{\mathrm{G}}, \varepsilon_{\mathrm{W}}, \varepsilon_{\mathrm{V}}$	0.9, 0.93, 0.92, 0.96
Rural Overall Albedo	α_{rur}	0.1
Rural Emissivity	$\varepsilon_{\mathrm{rur}}$	0.93
Rural Aerodynamic Roughness Length [m]	$\mathrm{z_0}$	0.1
Average boundary layer height [m]	$\mathrm{H_{bl}}$	2000
Vertical resolution [m]	$\Delta \mathrm{z}$	2
Canyon axis orientation °N	θ_{can}	-45

and fractional bias (FB) are calculated to perform a quantitative error analysis

$$NMSE = \frac{\sum_{i=1}^{n}(O_i - M_i)^2}{(\sum_{i=1}^{n} O_i)(\sum_{i=1}^{n} M_i)}, \tag{20}$$

$$FB = \frac{\sum_{i=1}^{n} O_i - \sum_{i=1}^{n} M_i}{0.5(\sum_{i=1}^{n} O_i + \sum_{i=1}^{n} M_i)}, \tag{21}$$

where O_i and M_i are the field observations and results from the VCWG model, respectively (see Table 2). While FB is a measure of the shift between the observed and predicted quantities, NMSE is a measure of the spread between observed and predicted quantities. For a perfect model, FB and NMSE are both equal to zero. As shown in Fig. 7, the potential temperature profiles show a typical diurnal cycle of atmospheric stability, starting with strongly stable condition after midnight (0000 LST) and persisting until just before the sunrise. Subsequently, the potential temperature profiles tend to neutral and unstable conditions as the sun rises (0800 LST). During the daytime, the urban surfaces are absorbing solar radiation causing the atmosphere at the lower levels to rise in temperature resulting in strongly unstable conditions (1200 LST and 1600 LST). As the sun sets in the late afternoon, the urban surfaces are cooled, which result in weakly unstable and then again stable conditions for the following day. The temperature difference between the urban (inside canyon) and rural areas, which is known as Urban Heat Island (UHI), shows that UHI hits a peak in the late afternoon for the day of interest with an average of $+1.0$ K, which is in reasonable agreement with the study by Aliabadi et al. (2019) predicting an average UHI of $+0.7$ K in August 2017. The

https://doi.org/10.5194/gmd-2019-176
Preprint. Discussion started: 27 August 2019

Geoscientific Model Development Discussions

VCWG follows the trend of the measured potential temperature within and above the canyon, particularly during the daytime. The error analysis shows that the average $\mathrm{NMSE}_{\overline{\Theta}}$ and $\mathrm{FB}_{\overline{\Theta}}$ are quantified as 0.002 and 0.051, respectively.

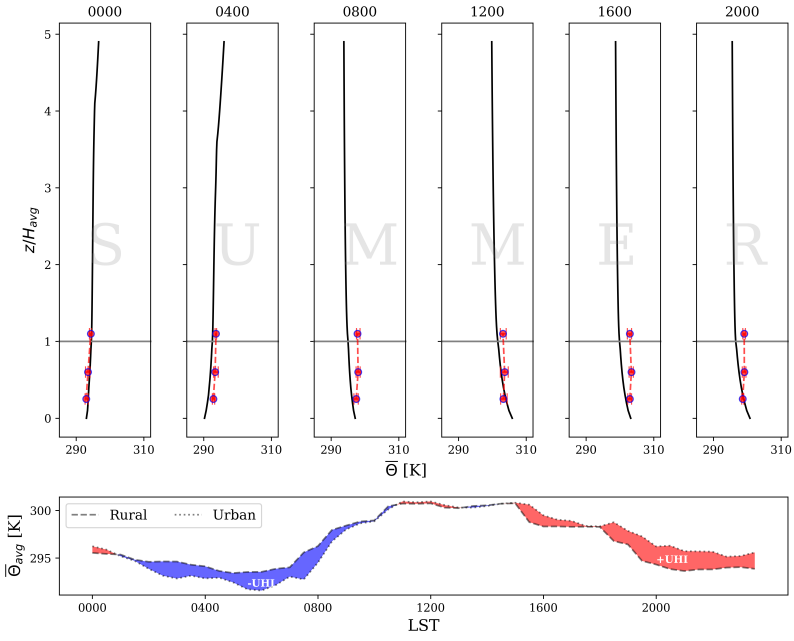

Figure 7. Comparison between the field measurements and the VCWG prediction of potential temperature profiles in the urban site; diurnal variation of UHI.

As shown in Fig. 8, the vertical profile of mean horizontal wind speed obtained from the VCWG shows reasonable agreement with the field data and it is always within the error bar (5th and 95th hourly percentiles) at different heights. The effects of urban obstacles, which induce drag and substantially reduce wind speed within the built-up area, are captured by the model. It has been proposed that the oncoming boundary layer and the shear layer developing at the roof level significantly contribute in mass and momentum exchange between the in-canyon and above-canyon atmosphere (Kang and Sung, 2009; Perret and Savory, 2013). This shear layer is characterized by highly turbulent flow making the measurements and simulations more challenging (Salizzoni et al., 2011; Perret and Savory, 2013). Figure 8 exhibits that the VCWG deviates predicting the average wind speeds at this height, but there is an overall reasonable agreement with the measurements, with an average NMSE and FB of 0.062 and 0.112, respectively (see Table 2).

As discussed in Sect. 2.2, the relative humidity was only measured at the street level. Figure 9 compares the 30-min average specific humidity measured in the field with the mean specific humidity within the canyon obtained from the VCWG. The vertical variation of $\overline{\mathrm{Q}}$ in the canyon is not significant (not shown here). From error analysis, small average values of both $\mathrm{NMSE}_{\overline{\mathrm{Q}}}$ and $\mathrm{FB}_{\overline{\mathrm{Q}}}$, 0.012 and 0.074 respectively, show an acceptable agreement with the experimental data.

https://doi.org/10.5194/gmd-2019-176
Preprint. Discussion started: 27 August 2019

Geoscientific Model Development Discussions
Open Access
EGU

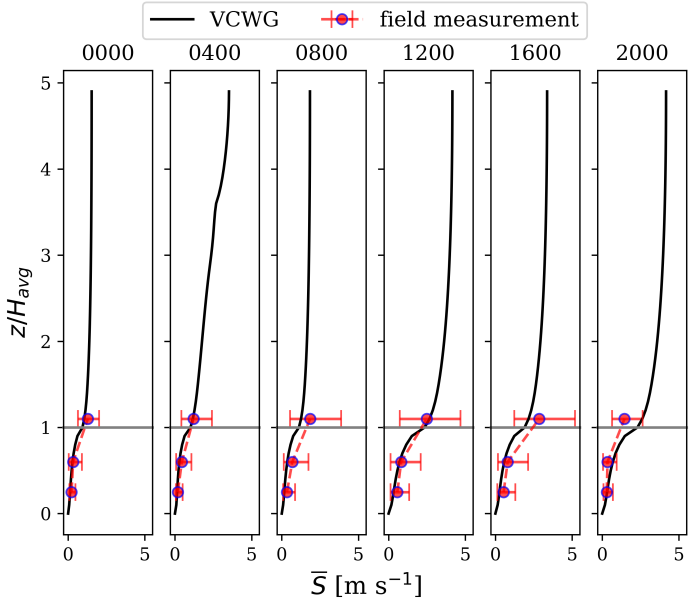

Figure 8. Comparison between the field measurements and the VCWG prediction of mean horizontal wind speed profiles in the urban site.

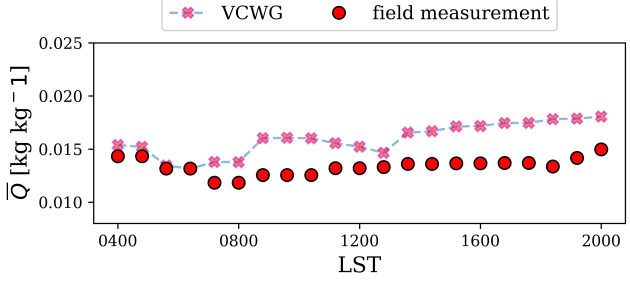

Figure 9. Comparison between the field measurements and the VCWG prediction of specific humidity in the urban site.

https://doi.org/10.5194/gmd-2019-176
Preprint. Discussion started: 27 August 2019

Geoscientific Model Development Discussions
Open Access
EGU

Table 2. Normalized Mean Square Error (NMSE) and Fractional Bias (FB) for potential temperature, mean horizontal wind speed, and specific humidity in the urban site.

Parameter →	Temperature		Horizontal wind speed		Specific humidity	
LST ↓	$\mathrm{NMSE}_{\overline{\Theta}}$	$\mathrm{FB}_{\overline{\Theta}}$	$\mathrm{NMSE}_{\overline{S}}$	$\mathrm{FB}_{\overline{S}}$	$\mathrm{NMSE}_{\overline{Q}}$	$\mathrm{FB}_{\overline{Q}}$
0000	0.002	−0.071	0.024	0.221	-	-
0400	0.003	0.085	0.010	0.144	-	-
0800	0.003	0.097	0.094	0.468	0.002	−0.045
1200	0.000	0.025	0.007	0.043	0.007	0.085
1600	0.003	0.096	0.047	0.327	0.006	0.080
2000	0.002	0.075	0.191	−0.532	0.031	0.175
Overall	0.002	0.051	0.062	0.112	0.012	0.074

Table 3. List of input parameters for the simulations designed to explore various urban configurations (The average foliage density of LAD_1, LAD_2, LAD_3 options are presented.). The latitude, longitude, aerodynamic roughness length scale, albedos, emissivities, building type, vertical resolution, and canyon axis orientation for these explorations are the same as in Table 1.

Case Studies →	Urban Configuration		Vegetation	Seasons
Input Parameters ↓	$\lambda_{p1}, \lambda_{p2}, \lambda_{p3}$	$\lambda_{f1}, \lambda_{f2}, \lambda_{f3}$	$\mathrm{LAD}_1, \mathrm{LAD}_2, \mathrm{LAD}_3$	$\mathrm{SE}_s, \mathrm{SE}_w$
Season	Summer	Summer	Summer	Summer,Winter
λ_p	0.25, 0.36, 0.44	0.44	0.44	0.44
λ_f	0.55	0.42, 0.55, 0.69	0.55	0.55
$\mathrm{H_{avg}}[\mathrm{m}]$	20	15, 20, 25	20	20
Average of Leaf Area Density (LAD) profile $[\mathrm{m^2 m^{-3}}]$	0.048	0.048	0.039, 0.048, 0.104	0.048

3.2 Model Exploration

The VCWG performance is assessed by evaluating the model performance as a function of the urban configurations (λ_p, λ_f, LAD), different seasons (SE), different climate zones (CZ), and time series analysis. More details on the explorations are provided in the subsequent sections and Tables 3 and 4. Such analyses will provide more information on spatiotemporal variation of the atmospheric meteorological states and reveal the complexity of urban microclimate modelling. Additionally, the potentials and limitations of VCWG will be discussed.

3.2.1 Urban Plan and Frontal Area Densities

In urban canopy modelling, two parameters often used to describe building and canyon geometries are plan area density (λ_p), which is the ratio of the total plan area of the buildings to the total urban earth surface area, and the frontal area density (λ_f),

https://doi.org/10.5194/gmd-2019-176
Preprint. Discussion started: 27 August 2019

Geoscientific Model Development Discussions

which is the ratio of the total frontal area (facing wind) to the total urban earth surface area. An urban area can be characterized with different types of land use, where each type may have different plan and frontal area densities, they can vary from high value in industrial districts to low values associated with the land used for public transportation (Wong et al., 2010). Any development in an urban area could be associated with changing λ_{p} and λ_{f}, which can alter the local climate in different ways such as air and surface temperatures, building energy consumption, and thermal and wind comfort levels (Coutts et al., 2007; Emmanuel and Steemers, 2018).

Three case studies λ_{p1}, λ_{p2}, and λ_{p3} with values of 0.25, 0.36, and 0.44, respectively, are explored to assess the model and see how the urban microclimate changes when the plan area density increases. The other parameters, which describe the cases, including the urban site (Guelph, Ontario, Canada), building dimensions, leaf area density profile, and the season that the VCWG was run, are listed in Table 3. Figure 10 shows typical nighttime and daytime profiles of potential temperature and mean horizontal wind speed in the urban area. Higher λ_{p} is associated with more urban surfaces allowing greater absorption of longwave and shortwave radiation and therefore higher level of building energy consumption for cooling, particularly during the day. It is depicted in Fig. 10 that the case with higher λ_{p} shows higher potential temperature profiles during the day and night. During the nighttime, the temperature difference between the cases is not as much as the daytime, however, still higher temperatures can be obtained when plan area density is higher. Additionally, more urban surfaces impose more drag and consequently reduce wind speed (see Fig. 10).

Further investigations are performed for different frontal area densities λ_{f}=0.42, 0.55, and 0.69, equivalent to the average building heights of 15, 20, and 25 m, respectively (see Table 3). At first glance, the cities with high-rise buildings are supposed to release more heat into the outdoor environment due to greater urban surfaces, but tall buildings can provide solar shading during the daytime and decrease temperature of the surfaces. As shown in Fig. 11, any increase in λ_{f} reduces potential temperature in the urban area during the day. However, due to the lack of shortwave radiation over nighttime and that urban surfaces are the main source of heat that can be released into the atmosphere, higher λ_{f} does not necessarily result in higher potential temperatures at nighttime. Moreover, increased frontal area density tends to increase surface roughness and consequently slow down wind speed, which can also be depicted in Fig. 11. The VCWG results are also consistent with previous studies in the literature (Coutts et al., 2007; Zajic et al., 2011; Santiago et al., 2014). The findings reported here highlight the careful considerations that need to be accounted for by city planners.

3.2.2 Leaf Area Density

Urban trees interact with the other urban elements by providing shade to reduce temperature of surfaces, removing the stored heat in the canyon substantially, and induce drag to reduce wind speed (Loughner et al., 2012; Krayenhoff et al., 2015; Redon et al., 2017). The capability of the VCWG to take into account these effects is assessed by investigating three case studies with LAD_1, LAD_2 and LAD_3 representing trees with low to high average foliage densities of 0.039, 0.048, and 0.104 $\mathrm{m^2 m^{-3}}$, respectively (see Table 3). The result is shown in Fig. 12. The cooling effect of the trees is evident when the average LAD of tree foliage increases from $0.039\ \mathrm{m^2 m^{-3}}$ to $0.104\ \mathrm{m^2 m^{-3}}$, resulting in a decrease of potential temperature within the canyon, particularly during the day when the shading effect of trees lowers the surface temperatures. Such effects not only can improve

https://doi.org/10.5194/gmd-2019-176
Preprint. Discussion started: 27 August 2019

Geoscientific Model Development Discussions

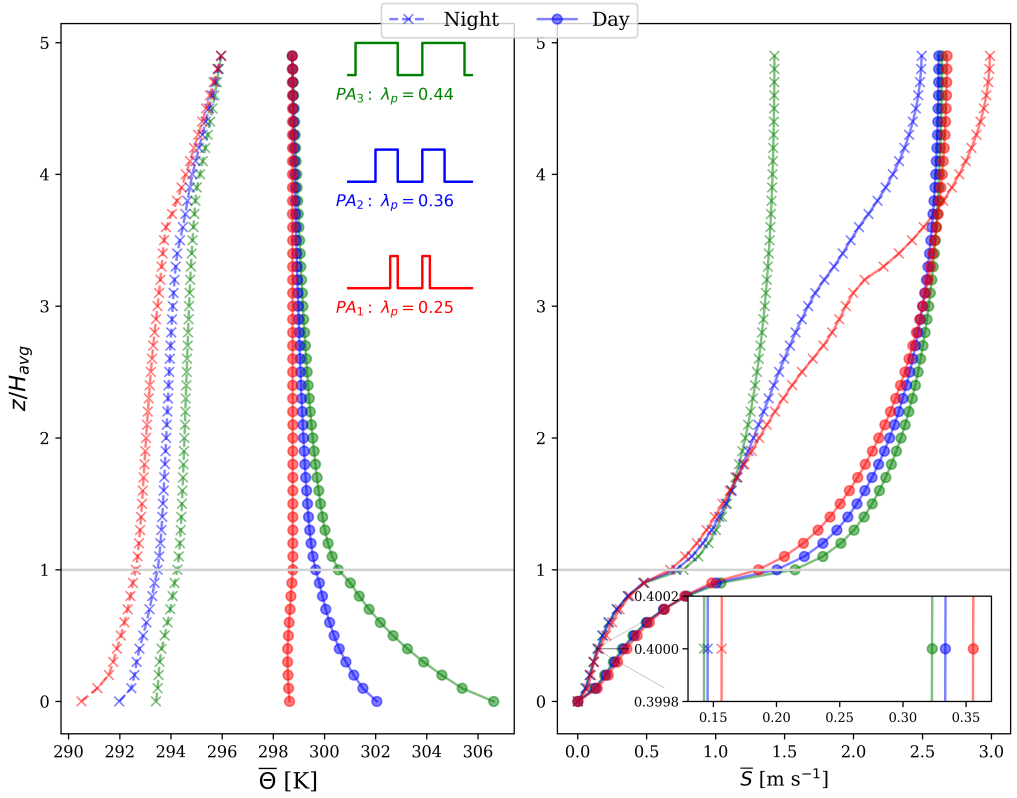

Figure 10. Effect of plan area density λ_p on the profiles of potential temperature and mean horizontal wind speed during nighttime (0400 LST) and daytime (1400 LST).

thermal comfort at the pedestrian level, but also reduce the building energy consumption in the Summertime (Souch and Souch, 1993; Akbari et al., 2001). On the other hand, the urban trees are thought to be a sink of momentum and kinetic energy by exerting drag and damping the flow fluctuations (Giometto et al., 2017; Yuan et al., 2017). This effect cannot be modelled very well by VCWG, which predicts the same level of wind speed within the canyon at all LADs. The analysis obtained from this exploration is in reasonable agreement with previous works (Souch and Souch, 1993; Loughner et al., 2012; Giometto et al., 2017; Yuan et al., 2017). Trees are recognized to be essential urban elements to moderate extreme wind speeds and heat waves, particularly during the warm season.

3.2.3 Seasonal Variations

In the context of urban development, there are no unique and pre-designed guidelines which can be extended to all built-up areas because careful considerations of geographical features and seasonal variations are required. For example, the type of urban vegetation, which is well suited for both warm and cold seasons in fulfilling thermal and wind comfort standards, can

https://doi.org/10.5194/gmd-2019-176
Preprint. Discussion started: 27 August 2019

Geoscientific Model Development Discussions
Open Access
EGU

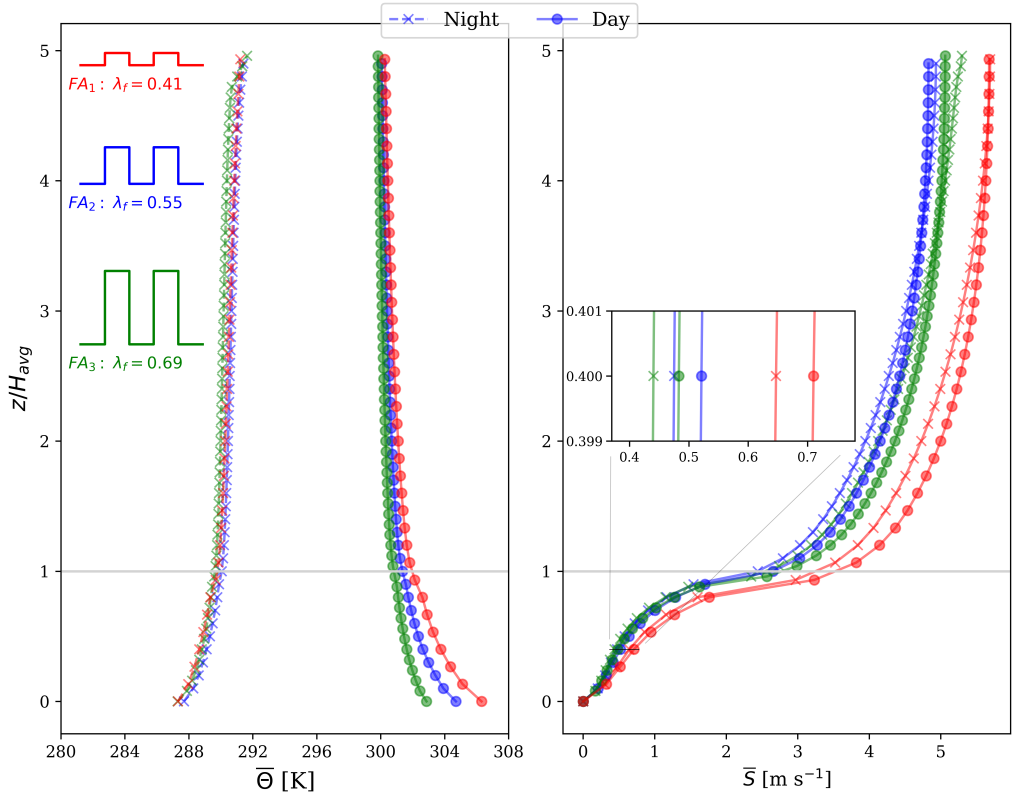

Figure 11. Effect of frontal area density λ_f on the profiles of potential temperature and mean horizontal wind speed during nighttime (0400 LST) and daytime (1400 LST).

be climate specific (Jamei et al., 2016). Winter is characterized by larger zenith angles and lower solar radiation received by the surfaces compared to the other seasons. In Winter, the temperature difference between indoor and outdoor environment is higher than the Summer, thus, seasonal variations can alter building energy consumption and UHI effects substantially (Bueno et al., 2011).

Figure 13 shows the VCWG results for the diurnal variations of potential temperature profiles in both rural and urban areas and the UHI for the Wintertime in Guelph, Canada. In the Winter, the urban boundary layer is almost always unstable, while the rural boundary layer is almost always stable or weakly stable due to the lack of significantly positive or negative heat flux at the surface in such cold weather. On the other hand, due to the dominance of building waste heat and the anthropogenic activities in the Wintertime, there is always heating in the urban area, which creates an unstable boundary layer coupled to a weakly stable rural boundary layer most of the time. The VCWG predicted positive UHI for the whole day, which is often observed during cold seasons depending on the climate zone (Cui and De Foy, 2012; Rasul et al., 2016; Yang and Bou-Zeid, 2018). The thermal comfort and energy savings advantages of UHI is now revealed in the Winter for cold climate zones, which

https://doi.org/10.5194/gmd-2019-176
Preprint. Discussion started: 27 August 2019

Geoscientific Model Development Discussions
Open Access
EGU

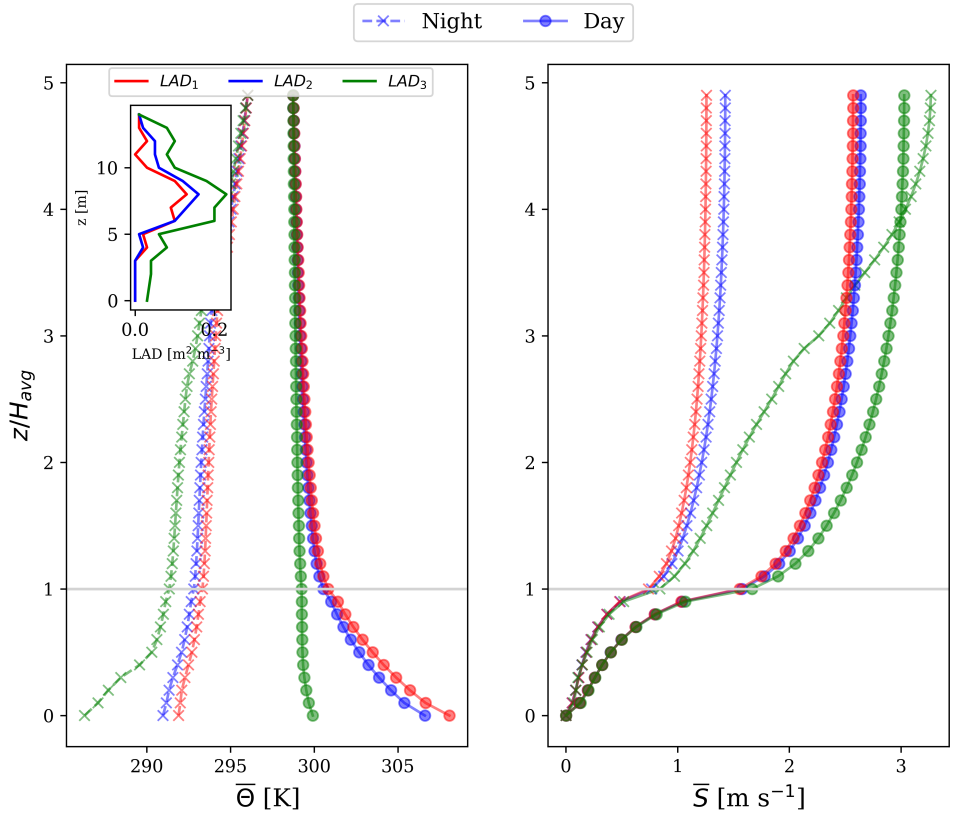

Figure 12. Effect of leaf area density profiles on the profiles of potential temperature and mean horizontal wind speed during nighttime (0400 LST) and daytime (1400 LST).

creates warmer cities and makes buildings less exposed to cold and consequently reduced building energy demand for heating (Santamouris et al., 2001; Oikonomou et al., 2012).

3.2.4 Other Climates

Generation of UHI is mainly attributed to the building material and geometry, sky view factor, cyclic factors, and anthropogenic heat. The process of urbanization increases heat storage in the city by trapping longwave radiation in the canyon by limiting the sky view factor, increasing anthropogenic heat fluxes, increasing absorption of shortwave radiation, and decreasing natural cooling due to removal of green spaces (Coutts et al., 2007; Rizwan et al., 2008). Thus, urban configuration, the Universal Transverse Mercator (UTM) zones, where each are exposed to a different solar path, and land use types mainly control intensity of UHI in different seasons. UHI could be observed during the daytime or nighttime, depending on the wind speed and seasonal

https://doi.org/10.5194/gmd-2019-176
Preprint. Discussion started: 27 August 2019

Geoscientific Model Development Discussions
Open Access
EGU

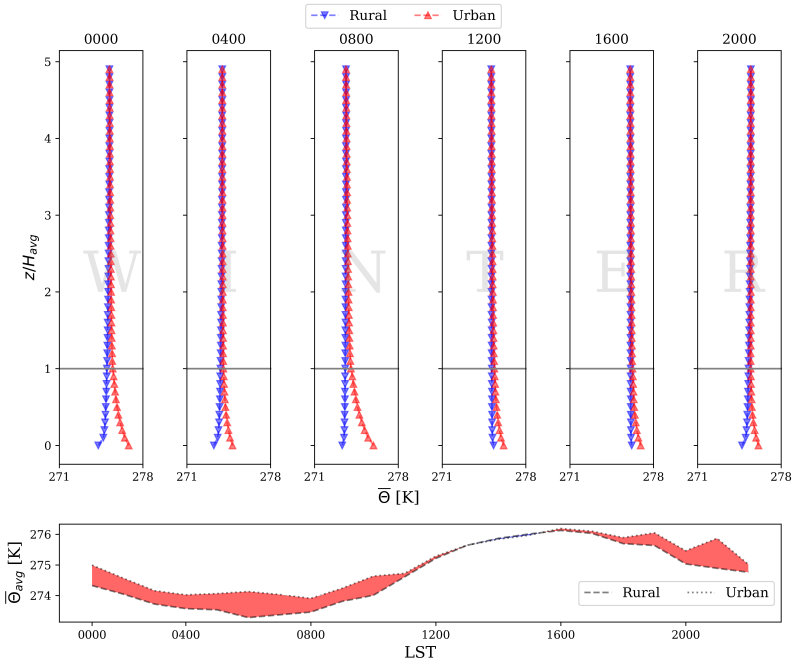

Figure 13. Diurnal variation of potential temperature profiles in the urban and rural areas in the Winter at Guelph, Canada, as predicted by VCWG.

time (Kłysik and Fortuniak, 1999) or types of urban land use (Siu and Hart, 2013), which signify spatial variation and temporal variation of UHI in a city.

The VCWG was further explored by predicting UHI in different cities with different climate zones including Buenos Aires CZ_{Bs} in December 1983, a city in the southern hemisphere with hot and humid climate, Tucson CZ_{TUS} in August 1967, which has a dry desert climate, Vancouver CZ_{VBC} in August 2011, representing a moderate oceanic climate, Osaka CZ_{OSA} in August 1996, with subtropical climate, and Copenhagen CZ_{CPH} in August 1999, representing cold and temperate climate. Input parameters for each case are detailed in Table 4. All simulations were conducted for one day of the month (see Fig. 14). The result shows about $+1.5$ K UHI for Buenos Aires during the night, which is consistent with a previous study measuring an average UHI of $+2.0$ K (Bejaran and Camilloni, 2003). The temperature difference between rural and urban areas in a dry and hot climate like Tucson is relatively higher with the average UHI value of $+2.5$ K, in agreement with a measured average UHI of $+2.1$ K (Comrie, 2000; Wang et al., 2016). In case of Vancouver, the VCWG predicted UHI from the afternoon to 0300LST and showed high intensity in the late afternoon. VCWG predicted a maximum UHI of $+1.8$ K in Vancouver, in agreement with measured value of $+1.4$ K (Runnalls, 1995; Lesnikowski, 2014; Ho et al., 2016). Case studies in Japan have reportedly obtained urban warming in large and developed cities such as Osaka, which is the interest in this study, and Tokyo in the afternoon (Leal Filho et al., 2017). This effect is also predicted by VCWG that showed the average UHI of $+1.0$ K, which is consistent with other studies measuring an average UHI of $+1.5$ K (Kusaka et al., 2012; Leal Filho et al., 2017). UHI

https://doi.org/10.5194/gmd-2019-176
Preprint. Discussion started: 27 August 2019

Geoscientific Model Development Discussions

Table 4. List of input parameters for the simulations designed to explore various climate zones. The aerodynamic roughness length scale, albedos, emissivities, building type, vertical resolution, and canyon axis orientation for these explorations are the same as in Table 1.

Case Studies →	Climate Zones				
Input Parameters ↓	CZ_{Bs}	CZ_{TUS}	CZ_{VBC}	CZ_{OSA}	CZ_{CPH}
Latitude °N	−34.82	32.12	49.20	34.78	55.63
Longitude °W	58.53	110.93	123.18	−135.45	−12.67
Season	Summer	Summer	Summer	Summer	Summer
λ_p	0.44	0.44	0.44	0.44	0.44
λ_f	0.82	0.55	0.55	0.55	0.55
$H_{avg}[m]$	30	20	20	20	20
Average of Leaf Area Density (LAD) profile $[m^2m^{-3}]$	0.048	0.048	0.048	0.048	0.048

in Copenhagen is reported to change between $+0.5$ and $+1.5$ K depending on the wind speed, which agrees well with the VCWG prediction of $+1.3$ K, as well as intensifying in the afternoon (Mahura et al., 2009).

3.2.5 Time Series Analysis

The VCWG was run for two weeks starting from 11 August 1967 in Tucson, where the EPW weather file is continuously available for two weeks. Hourly time series of urban and rural temperatures with the corresponding relative humidity, incoming direct and diffusive solar radiation from sky, and mean horizontal wind speed in the rural area are shown in Fig. 15. The model can capture the cyclic pattern of temperature that is affected by the other meteorological quantities. For example, UHI is mainly obtained during nighttime and urban cool island during daytime. In a mostly-cloudy day of 13 August 1967, less incoming radiation is associated with lower temperatures and a lower UHI compared to the other days. In a mostly-quiescent day of 21 August 1967 where wind speeds are lower, there is less turbulence mixing, and consequently more heat is trapped in the urban area that results in higher UHI.

4 Conclusions and Future Work

The Vertical City Weather Generator (VCWG) is an urban microclimate model designed to calculate vertical profiles of meteorological variables including potential temperature, wind speed, specific humidity, and turbulence kinetic energy in an urban area. The VCWG is composed of sub models for ingestion of urban parameters and meteorological variables in a rural area as boundary conditions and prediction of the meteorological variables in a nearby urban area, the building energy performance variables, and the short and longwave radiation transfer processes. VCWG combines elements of several previous models developed by Lee and Park (2008), Santiago and Martilli (2010), Bueno et al. (2014), Krayenhoff et al. (2014), Krayenhoff

https://doi.org/10.5194/gmd-2019-176
Preprint. Discussion started: 27 August 2019

Geoscientific Model Development Discussions

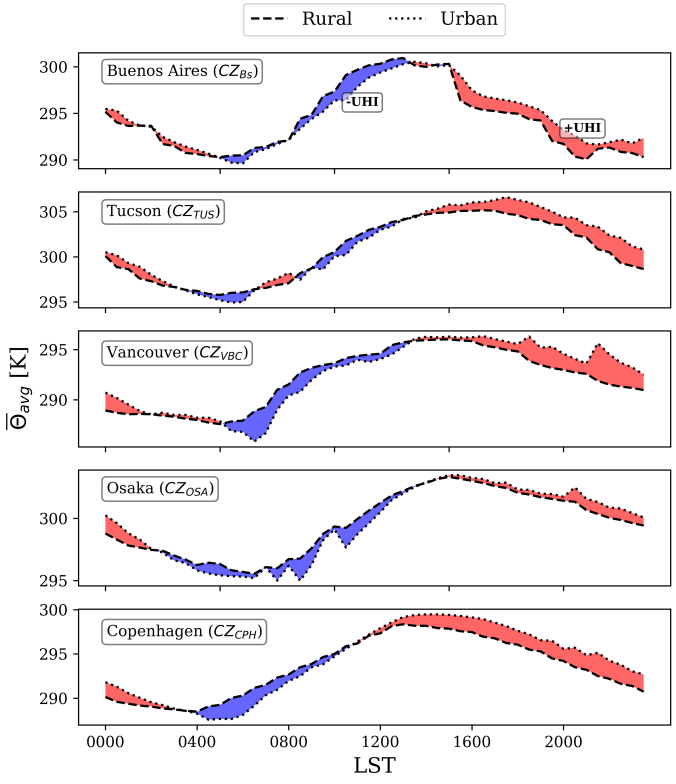

Figure 14. Diurnal variation of the average urban and rural temperatures in Buenos Aires $\mathrm{CZ_{Bs}}$, Tucson $\mathrm{CZ_{TUS}}$, Vancouver $\mathrm{CZ_{VBC}}$, Osaka $\mathrm{CZ_{OSA}}$, and Copenhagen $\mathrm{CZ_{CPH}}$ for a single day in Summer. Positive and negative UHIs are shown by red and blue shaded regions, respectively.

et al. (2015), and Redon et al. (2017) to generate a model with the ability to predict vertical profiles of urban meteorological variables, forced by rural measurements, and with feedback interaction with both building energy and radiation models.

To evaluate VCWG, a microclimate field campaign was held from 15 July 2018 to 5 September 2018, in Guelph, Canada. The data was collected at the University of Guelph main campus representing an urban site and in the Guelph Turfgrass Institute, which is an open space to be considered as a nearby rural site. In the urban site, temperature, wind velocity components, relative humidity, and solar radiation were measured. In the rural site, the temperature and relative humidity at 2 m as well as wind speed and direction at 10 m were provided from a weather station by the World Meteorological Organization (WMO) dataset. The results obtained from VCWG agreed reasonably well with the measurements and predicted a $+1.0$ K Urban Heat Island (UHI) with reasonable agreement to a measured value of $+0.7$ K in the previous year. Nevertheless, the before-sunrise UHI is not exactly reproduced, which is a current limitation of the model. The error analysis showed overall a Normalized Mean

https://doi.org/10.5194/gmd-2019-176
Preprint. Discussion started: 27 August 2019

Geoscientific Model Development Discussions
Open Access
EGU

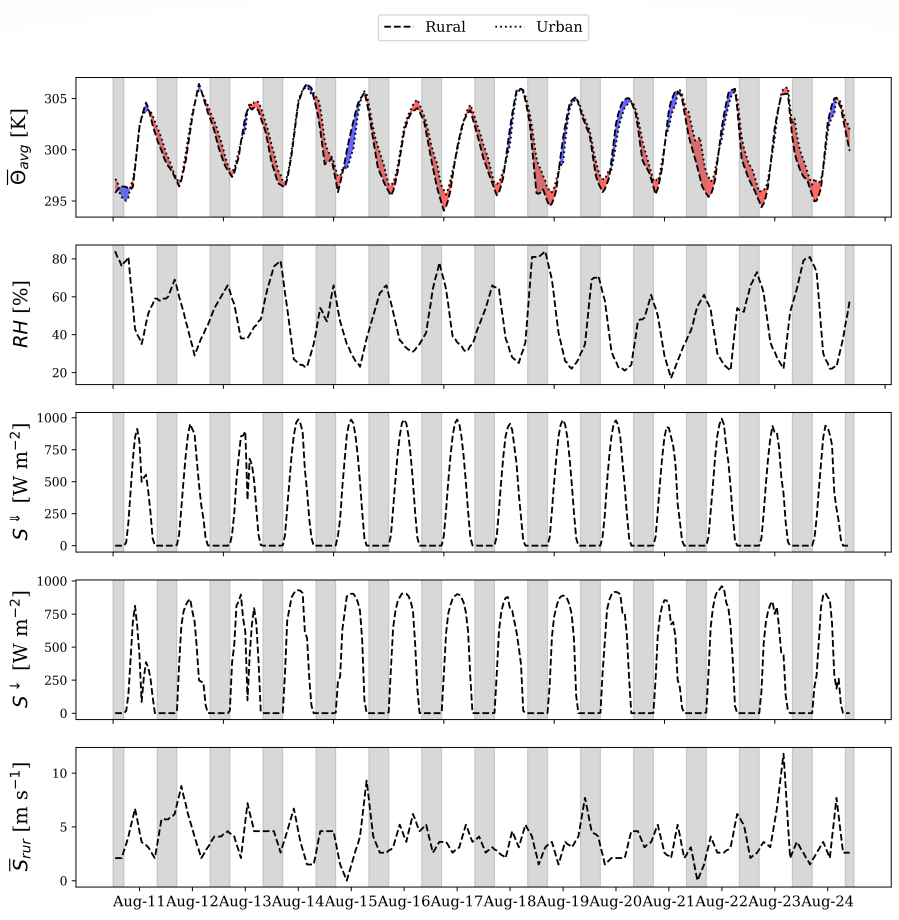

Figure 15. Hourly time series of rural and urban temperatures, rural relative humidity, rural incoming solar radiation, and rural mean horizontal wind speed from 11 August 1967 in Tucson, Arizona, USA; the shaded areas represent nighttime.

Square Error (NMSE) of 0.002, 0.062, and 0.012 and overall a Fractional Bias (FB) of 0.051, 0.112, and 0.074 for potential temperature, wind speed, and specific humidity, respectively.

The performance of the VCWG was further assessed by conducting five types of explorations for both nighttime and daytime urban microclimate. First, we investigated how the urban geometry, which is characterized by plan area density λ_p and frontal area density λ_f, could affect the urban microclimate. Any increase in λ_p was associated with higher air temperatures and reduced wind speeds within the urban canyon. On the other hand, a configuration with higher λ_f increased shading effects and consequently reduced daytime temperatures, but it increased nighttime temperatures due to more heat released from urban surfaces that was trapped in the canyon. The cooling effect of the urban vegetation was also evaluated by changing the Leaf Area Density (LAD) profiles within the canyon. Increasing the average LAD showed heat removal from the canyon alongside

https://doi.org/10.5194/gmd-2019-176
Preprint. Discussion started: 27 August 2019

Geoscientific Model Development Discussions

with lower wind speeds due to the drag induced by trees. Another exploration made in the Wintertime justified the ability of the VCWG to predict the urban microclimate in both cold and warm seasons. The result showed the expected diurnal variation of temperature profile in the urban site. The ability of the model to predict UHI in different cities with different climate zones was assessed. The case studies were Buenos Aires, Tucson, Vancouver, Osaka, and Copenhagen. Finally, VCWG was able to produce realistic urban temperatures when it was run continuously for two weeks in Tucson. All exploration results obtained from the VCWG were reasonably consistent with the previous studies in the literature, except for occasional underprediction of UHI in the early morning.

In this study, it was shown that the urban microclimate model VCWG can successfully extend the spatial dimension of the preexisting bulk flow (single-layer) urban microclimate models to one-dimension in the vertical direction, while it also considers the relationship of the urban microclimate model to the rural meteorological and the building energy conditions. The effect of the key urban elements such as building configuration, building energy systems, and vegetation were considered, but there is still opportunity to improve VCWG further. The urban site is simplified as blocks of buildings with symmetric and regular dimensions, which can be more realistically represented if more considerations were to be taken into account about nonuniform distribution of buildings dimensions. Future studies can also focus on improvement of flow field parameterization or including additional source/sink terms in the transport equations to model horizontal motions, eddies, and flow fluctuations in the urban area, which is realistically very three-dimensional and heterogenous. VCWG development can account for the spatial variation of urban microclimate in a computationally efficient manner independent of an auxiliary mesoscale model. This advantage is really important for urban planners, architects, and consulting engineers, to run VCWG operationally fast for many projects.

Code and data availability. The VCWG v1.0.0 is developed at the Atmospheric Innovations Research (AIR) Laboratory at the University of Guelph: http://www.aaa-scientists.com. The source code and the supporting environmental field monitoring data are available under GPL 3.0 licence: https://opensource.org/licenses/GPL-3.0 (last access: May 2019) and can be downloaded from https://www.zenodo.org/ with DOI: 10.5281/zenodo.3376792.

Appendix A

A1 Heat flux in the rural area

The net sensible heat fluxes at the surface level in the rural area can be decomposed into heat flux caused by vegetation, radiation flux absorbed by the surface, and the heat convection flux between the outer layer of soil and the atmosphere (see Eq. 5). The sensible heat flux from vegetation can be calculated as

$$Q_{Hveg,rur} = F_{veg} F_{lat,grass} (1 - \alpha_V) Q^{rec}_{rad,rur} \tag{A1}$$

https://doi.org/10.5194/gmd-2019-176
Preprint. Discussion started: 27 August 2019

Geoscientific Model Development Discussions

where F_{veg} is the fraction of the rural area covered by vegetation, $F_{lat,grass}$ is fraction of absorbed heat that is converted to an emitted latent heat flux, α_V is the albedo of the vegetation, and $Q^{rec}_{rad,rur}$ is the solar radiation flux received at the rural surface given in the weather file. The net solar radiation flux absorbed at the surface can calculated from

$$Q_{rad,rur} = ((1 - F_{veg})(1 - \alpha_{rur}) + F_{veg}(1 - \alpha_V))Q^{rec}_{rad,rur}, \tag{A2}$$

where α_{rur} is overall albedo of the rural. The albedos of the rural area are input parameters in VCWG.

A2 Source/Sink Term in the 1-D Model

The pressure and skin drags exerted on the flow in Eq.s 10 and 11 are formulated as follow (Krayenhoff et al., 2015)

$$D_x = \underbrace{\frac{1}{\rho}\frac{\partial \tilde{P}}{\partial x}}_{I} - \underbrace{\nu(\nabla^2 \tilde{U})}_{II}, \tag{A3}$$

$$D_y = \underbrace{\frac{1}{\rho}\frac{\partial \tilde{P}}{\partial y}}_{I} - \underbrace{\nu(\nabla^2 \tilde{V})}_{II}, \tag{A4}$$

where term I represents dispersive pressure variation (form drag) induced by vegetation and building and term II represents the dispersive viscous dissipation (skin drag) induced by horizontal surfaces. The former can be parameterized as below

$$\frac{1}{\rho}\frac{\partial \tilde{P}}{\partial x} = -\left(B_D C_{DBv} + LAD\Omega C_{DV}\right)\overline{U}_{expl}\overline{U}, \tag{A5}$$

$$\frac{1}{\rho}\frac{\partial \tilde{P}}{\partial y} = -\left(B_D C_{DBv} + LAD\Omega C_{DV}\right)\overline{V}_{expl}\overline{V}, \tag{A6}$$

where B_D is sectional building area density, C_{DBv} is sectional drag coefficient in the presence of trees, LAD is leaf area density in the canyon, Ω is clumping factor, C_{DV} is the drag coefficient for tree foliage, and $\overline{U}_{expl}$ and $\overline{V}_{expl}$ are wind velocity components in x and y directions from a previous numerical solution, respectively, which are assumed explicitly as constants to linearize the system of equations to be solved. The skin drag can be parameterized as follow

$$\nu(\nabla^2 \tilde{U}) = -c_d f_m \overline{U}_{expl}\overline{U}, \tag{A7}$$

$$\nu(\nabla^2 \tilde{V}) = -c_d f_m \overline{V}_{expl}\overline{V}, \tag{A8}$$

where c_d is skin drag coefficient and f_m is a function of stability from Louis (1979).

The terms related to wake production S_{wake} and dissipation rate ε in Eq. 13 can be parameterized as

$$S_{wake} = \left(B_D C_{DBv} + LAD\Omega C_{DV}\right)\overline{U}^3_{expl}, \tag{A9}$$

$$\varepsilon = C_\varepsilon \frac{k^{\frac{3}{2}}}{\ell_{\varepsilon,dissip}}, \tag{A10}$$

where Ω is clumping factor, C_ε is a model constant and $\ell_{\varepsilon,dissip}$ is a dissipation length scale optimized using CFD.

https://doi.org/10.5194/gmd-2019-176
Preprint. Discussion started: 27 August 2019

Geoscientific Model Development Discussions

The heat source/sink terms, terms in Eq. 14, caused by roof ($S_{\Theta R}$) and ground ($S_{\Theta G}$) are calculated based on the study by Louis (1979) and the heat flux from the wall ($S_{\Theta W}$) is formulated in Martilli et al. (2002). The two other heat terms can be parameterized as below

$$S_{\Theta A} = \frac{4\rho_{abs}k_{air}}{\rho C_p v_L}\left[(1-\lambda_p)L_A\right], \tag{A11}$$

$$S_{\Theta V} = \frac{2g_{Ha}c_{PM}}{\rho C_p v_L}\left[LAD(1-\lambda_p)(\overline{\Theta}_V - \overline{\Theta})\right], \tag{A12}$$

where L_A is the absorbed flux density of longwave radiation in the canyon, ρ_{abs} is the density of absorbing molecules, k_{air} is their mass extinction cross section, v_L=$(1-\lambda_p)$ is the fraction of total volume that is outdoor air, g_{Ha} is conductance for heat, c_{PM} is the molar heat capacity for the air, and $\overline{\Theta}_V$ is the temperature of tree foliage.

In the humidity equation, the source/sink term can be calculated using the following equation

$$S_{QV} = \frac{\Lambda_M g_v \Omega}{\rho \Lambda v_L}\left[LAD(1-\lambda_p)(s[\overline{\Theta}_V - \overline{\Theta}]) + \frac{D}{P}\right] \tag{A13}$$

where Λ_M is molar latent heat of vaporization, g_v is the average surface and boundary-layer conductance for humidity for the whole leaf, D is the vapour deficit of the atmosphere, and P is atmospheric pressure.

A3 Building Heat Exchanges

The heat fluxes in Eq. 17 can be parameterized as bellow

$$\Sigma Q_{cv,i} = \Sigma h_i A_i (T_{si} - T_{in}) \tag{A14}$$

$$Q_{inf/exf} = \dot{m}_{inf/exf} C_p (T_{out} - T_{in}) \tag{A15}$$

$$Q_{sys} = \dot{m}_{sys} C_p (T_{supp} - T_{in}) \tag{A16}$$

where h_i and A_i are heat convection coefficient and surface area of indoor elements such as windows and ceiling. T_{si} is the temperature of inner layer of elements, T_{in} is indoor temperature, T_{out} is the outdoor temperature averaged over building height, T_{supp} is supply temperature, $\dot{m}_{inf/exf}$ is mass flow rate of infiltration/exfiltration, and $\dot{m}_{sys}$ is mass flow rate of the HVAC system.

A4 Longwave and Shortwave Radiation

For shortwave radiation, infinite reflections are considered. The total absorbed shortwave radiation by each urban element can be calculated by adding the first absorption of shortwave radiation before any reflection to the radiation received as a result of

https://doi.org/10.5194/gmd-2019-176
Preprint. Discussion started: 27 August 2019

Geoscientific Model Development Discussions

infinite reflections with the other elements. The following equations have been developed by Redon et al. (2017)

$$S_S = \Psi_{SG}\tau_{SG}G_\infty + \Psi_{SW}\tau_{SW}W_\infty + \Psi_{ST}\delta_T T_\infty \tag{A17}$$

$$S_G = S_G^0 + (1-\alpha_G)\left[\Psi_{GW}\tau_{GW}W_\infty + c_{GT}\Psi_{GT}\delta_t T_\infty\right] \tag{A18}$$

$$S_{W_i} = S_W^0 + (1-\alpha_W)\left[\Psi_{WG}\tau_{WG}G_\infty + \Psi_{WW}\tau_{WW}S_{W_j} + c_{WT}\Psi_{WT}\delta_T T_\infty\right] \tag{A19}$$

$$S_T = \frac{1}{\delta_T}\left[(S^{\Downarrow} + S^{\downarrow}) - (S_S + S_G + \frac{2H_{avg}}{w}S_W)\right] \tag{A20}$$

where the subscripts 'S', 'G', 'W', and 'T' represent sky, ground, wall, and tree respectively. The superscript '0' signifies the before-reflection absorption of shortwave radiation. The view factor between two urban elements is shown by Ψ with the suitable subscripts (e.g., Ψ_{GW} represent the view factor between ground and wall). The total shortwave radiation reflected by ground, wall, and trees are shown by G_∞, W_∞, and T_∞, respectively. $S^{\Downarrow}$ is direct incoming solar radiation, $S^{\downarrow}$ is diffusive incoming solar radiation ($S^{\Downarrow}$ and $S^{\downarrow}$ are both obtained from the input weather file), c_{GT} is a model constant, τ_{ij} is radiative transmissivity between two elements (e.g. i=G and j=W), w is street width, H_{avg} is average building height, and δ_T is fraction of road surface vegetation. The shading effect of trees are considered in the formulation of transmissivity (Lee and Park, 2008).

For longwave radiation, only one reflection is considered. The net longwave radiation received by the urban surfaces can be computed as (Lee and Park, 2008)

$$\begin{aligned} L_W =& \tau_{SW}\varepsilon_W\Psi_{SW}L_S + \tau_{WW}\varepsilon_W^2(1-2\Psi_{SW})\sigma T_W^4 + \tau_{GW}\varepsilon_W\Psi_{SW}L_G^{\uparrow} + \tau_{SG}\tau_{GW}(1-\varepsilon_G)\Psi_{SW}\Psi_{SG}L_S \\ &+ \tau_{WW}\varepsilon_W(1-\varepsilon_W)(1-2\Psi_W)^2\sigma T_W^4 + \tau_{SW}\tau_{WW}(1-\varepsilon_W)\Psi_{SW}(1-2\Psi_{SW})L_S \\ &+ \tau_{WG}\tau_{GW}(1-\varepsilon_G)\varepsilon_W\Psi_{SW}(1-\Psi_{SG})\sigma T_W^4 + \tau_{WW}^2\varepsilon_W(1-\varepsilon_W)(1-2\Psi_{SW})^2\sigma T_W^4 \\ &+ \tau_{GW}\tau_{WW}(1-\varepsilon_W)\Psi_{SW}(1-2\Psi_{SW})L_G^{\uparrow} + L_T^{G\uparrow} - \varepsilon_W\sigma T_W^4 \end{aligned} \tag{A21}$$

$$\begin{aligned} L_G =& \tau_{SG}\varepsilon_G\Psi_{SG}L_S + \tau_{WG}\varepsilon_W\varepsilon_G(1-\Psi_{SG})\sigma T_W^4 + \tau_{SW}\tau_{WG}(1-\varepsilon_W)\Psi_{SW}(1-\Psi_{SG})L_S \\ &+ \tau_{WW}\tau_{WG}\varepsilon_W(1-\varepsilon_W)(1-\Psi_{SG})(1-2\Psi_{SW})\sigma T_W^4 + \tau_{GW}\tau_{WG}(1-\varepsilon_W)\Psi_{SW}(1-\Psi_{SG})L_G^{\uparrow} + (1-\delta_T)L_T^{G\uparrow} - \varepsilon_G\sigma T_G^4 \end{aligned} \tag{A22}$$

$$L_T = \frac{1}{\sigma_T}\left[L_S + \frac{2H_{avg}}{w}L_W^{\uparrow} + L_G^{\uparrow} + \sigma_T L_T^{T\uparrow} - \frac{2H_{avg}}{w}L_W^{\downarrow} - L_G^{\downarrow} - L_S - \sigma_T L_T^{\uparrow}\right] \tag{A23}$$

where the upward and downward arrows indicate emitted and absorbed longwave radiation from and by the surface of interest, respectively. L_S is radiative flux emitted from the atmosphere, σ_T is leaf aspect ratio, T_W is wall temperature and T_G is ground temperature. The readers are invited to refer to the study by Lee and Park (2008) for more details on the parameterization of longwave radiation.

Author contributions. MM wrote the paper with significant conceptual input from ESK and AAA and critical feedback from all co-authors. BD, AN, MKN, and MRN operated the instruments in the field and partially analyzed resulting data. BB and LKN developed the base Urban

https://doi.org/10.5194/gmd-2019-176
Preprint. Discussion started: 27 August 2019

Weather Generator (UWG) program in MATLAB. CM and SV translated UWG from MATLAB to Python. ESK implemented parameterizations for trees in the one-dimensional vertical diffusion model for the urban climate. NN and ESK have improved the one-dimensional vertical diffusion model for the urban climate based on large-eddy simulations. MM and AAA developed the Vertical City Weather Generator (VCWG) program in Python by integrating various modelling components developed by BB, LKN, CM, SV, ESK, and NN.

Competing interests. The authors declare that they have no conflict of interest.

Acknowledgements. The authors are indebted to Steve Nyman, Chris Duiker, Peter Purvis, Manuela Racki, Jeffrey Defoe, Joanne Ryks, Ryan Smith, James Bracken, and Samantha French at the University of Guelph, who helped with the campaign logistics. Special credit is directed toward Amanda Sawlor, Esra Mohamed, Di Cheng, Randy Regan, Margaret Love, Angela Vuk, and Carolyn Dowling-Osborn at the University of Guelph for administrative support. The computational platforms were set up with the assistance of Jeff Madge, Joel Best, and Matthew Kent at the University of Guelph. The authors thank Alberto Martilli at Centre for Energy, Environment and Technology (CIEMAT) in Madrid, Spain, who developed and shared the one-dimensional vertical diffusion model for the urban climate. The authors also thank William D. Lubitz for providing a mini SOnic Detection And Ranging (SODAR) instrument and three ultrasonic anemometers for the field campaign.

This work was supported by the University of Guelph through the International Graduate Tuition Scholarship (IGTS) for the lead author; Philanthropic contributions from Professor Edward McBeans's Foundation toward acquisition of experimental equipment; Discovery Grant program (401231) from the Natural Sciences and Engineering Research Council (NSERC) of Canada; Government of Ontario through the Ontario Centres of Excellence (OCE) under the Alberta-Ontario Innovation Program (AOIP) (053450); and Emission Reduction Alberta (ERA) (053498). OCE is a member of the Ontario Network of Entrepreneurs (ONE).

https://doi.org/10.5194/gmd-2019-176
Preprint. Discussion started: 27 August 2019

Geoscientific Model Development Discussions

References

Adnot, J., Riviere, P., Marchio, D., Becirspahic, S., Lopes, C., Blanco, I., Perez-Lombard, L., Ortiz, J., Papakonstantnou, N., Doukas, P., et al.: Energy efficiency and certification of central air conditioners (EECCAC), Study for the DG Transportation-Energy (DGTREN) of the Commission of the EU, Paris, 2003.

Akbari, H.: Energy Saving Potentials and Air Quality Benefits of Urban Heat Island Mitigation, 2005.

Akbari, H., Pomerantz, M., and Taha, H.: Cool surfaces and shade trees to reduce energy use and improve air quality in urban areas, Sol. Energy, 70, 295–310, 2001.

Aliabadi, A. A., Staebler, R. M., de Grandpré, J., Zadra, A., and Vaillancourt, P. A.: Comparison of estimated atmospheric boundary layer mixing height in the Arctic and southern Great Plains under statically stable conditions: experimental and numerical aspects, Atmos.-Ocean, 54, 60–74, 2016a.

Aliabadi, A. A., Staebler, R. M., Liu, M., and Herber, A.: Characterization and parametrization of Reynolds stress and turbulent heat flux in the stably-stratified lower Arctic troposphere using aircraft measurements, Bound.-Layer Meteorol., 161, 99–126, 2016b.

Aliabadi, A. A., Krayenhoff, E. S., Nazarian, N., Chew, L. W., Armstrong, P. R., Afshari, A., and Norford, L. K.: Effects of roof-edge roughness on air temperature and pollutant concentration in urban canyons, Bound.-Lay. Meteorol., 164, 249–279, 2017.

Aliabadi, A. A., Moradi, M., Clement, D., Lubitz, W. D., and Gharabaghi, B.: Flow and temperature dynamics in an urban canyon under a comprehensive set of wind directions, wind speeds, and thermal stability conditions, Environ. Fluid Mech., 19, 1–29, 2019.

Armson, D., Stringer, P., and Ennos, A.: The effect of tree shade and grass on surface and globe temperatures in an urban area, Urban For. Urban Gree., 11, 245–255, 2012.

Balogun, A. A., Tomlin, A. S., Wood, C. R., Barlow, J. F., Belcher, S. E., Smalley, R. J., Lingard, J. J. N., Arnold, S. J., Dobre, A., Robins, A. G., Martin, D., and Shallcross, D. E.: In-street wind direction variability in the vicinity of a busy intersection in central London, Bound.-Lay. Meteorol., 136, 489–513, 2010.

Bejaran, R. and Camilloni, I.: Objective method for classifying air masses: an application to the analysis of Buenos Aires'(Argentina) urban heat island intensity, Theor. Appl. Climatol., 74, 93–103, 2003.

Blocken, B.: Computational Fluid Dynamics for urban physics: Importance, scales, possibilities, limitations and ten tips and tricks towards accurate and reliable simulations, Build. Environ., 91, 219–245, 2015.

Bornstein, R. D.: The two-dimensional URBMET urban boundary layer model, J. Appl. Meteorol., 14, 1459–1477, 1975.

Britter, R. E. and Hanna: Flow and Dispersion in Urban Areas, Annu. Rev. Fluid Mech, 35, 469–496, 2003.

Broadbent, A. M., Coutts, A. M., Nice, K. A., Demuzere, M., Krayenhoff, E. S., Tapper, N. J., and Wouters, H.: The Air-temperature Response to Green/blue-infrastructure Evaluation Tool (TARGET v1. 0): an efficient and user-friendly model of city cooling, Geosci. Model Dev., 12, 785–803, 2019.

Bueno, B., Norford, L. K., Pigeon, G., and Britter, R.: Combining a detailed building energy model with a physically-based urban canopy model, Bound.-Lay. Meteorol., 140, 471–489, 2011.

Bueno, B., Norford, L. K., Hidalgo, J., and Pigeon, G.: The urban weather generator, J. Build. Perf. Simulat., 6, 269–281, 2012a.

Bueno, B., Pigeon, G., Norford, L. K., Zibouche, K., and Marchadier, C.: Development and evaluation of a building energy model integrated in the TEB scheme, Geosci. Model Dev., pp. 433–448, 2012b.

Bueno, B., Roth, M., Norford, L. K., and Li, R.: Computationally efficient prediction of canopy level urban air temperature at the neighbourhood scale, Urban Climate, 9, 35–53, 2014.

https://doi.org/10.5194/gmd-2019-176
Preprint. Discussion started: 27 August 2019

C. S. B. Grimmond, M. Best, J. B.: Urban Surface Energy Balance Models: Model Characteristics and Methodology for a Comparison Study. In: Baklanov A., Sue G., Alexander M., Athanassiadou M. (eds) Meteorological and Air Quality Models for Urban Areas, McGraw-Hill Inc., New York, 3rd edn., 2009.

Chen, F., Kusaka, H., Bornstein, R., Ching, J., Grimmond, C. S. B., Grossman-Clarke, S., Loridan, T., Manning, K. W., Martilli, A., Miao, S., Sailor, D., Salamanca, F. P., Taha, H., andX. Wang, M. T., Wyszogrodzki, A. A., and Zhang, C.: The integrated WRF/urban modelling system: development, evaluation, and applications to urban environmental problems, Int. J. Climatol., 31, 273–288, 2011.

Chin, H.-N. S., Leach, M. J., Sugiyama, G. A., Leone Jr, J. M., Walker, H., Nasstrom, J., and Brown, M. J.: Evaluation of an urban canopy parameterization in a mesoscale model using VTMX and URBAN 2000 data, Mon. Weather Rev., 133, 2043–2068, 2005.

Coceal, O. and Belcher, S.: A canopy model of mean winds through urban areas, Q. J. R. Meteorol. Soc., 130, 1349–1372, 2004.

Comrie, A. C.: Mapping a wind-modified urban heat island in Tucson, Arizona (with comments on integrating research and undergraduate learning), B. Am. Meteorol. Soc., 81, 2417–2432, 2000.

Conry, P., Fernando, H., Leo, L., Sharma, A., Potosnak, M., and Hellmann, J.: Multi-scale simulations of climate-change influence on Chicago Heat Island, in: ASME 2014 4th Joint US-European Fluids Engineering Division Summer Meeting collocated with the ASME 2014 12th International Conference on Nanochannels, Microchannels, and Minichannels, pp. V01DT28A007–V01DT28A007, American Society of Mechanical Engineers, 2014.

Coutts, A. M., Beringer, J., and Tapper, N. J.: Impact of increasing urban density on local climate: Spatial and temporal variations in the surface energy balance in Melbourne, Australia, J. Appl. Meteorol. Clim., 46, 477–493, 2007.

Cui, Y. Y. and De Foy, B.: Seasonal variations of the urban heat island at the surface and the near-surface and reductions due to urban vegetation in Mexico City, J. Appl. Meteorol. Clim., 51, 855–868, 2012.

De Munck, C., Pigeon, G., Masson, V., Meunier, F., Bousquet, P., Tréméac, B., Merchat, M., Poeuf, P., and Marchadier, C.: How much can air conditioning increase air temperatures for a city like Paris, France?, Int. J. Climatol., 33, 210–227, 2013.

Dupont, S., Otte, T. L., and Ching, J. K. S.: Simulation of meteorological fields within and above urban and rural canopies with a mesoscale model, Bound.-Lay. Meteorol., 113, 111–158, 2004.

Emmanuel, R. and Steemers, K.: Connecting the realms of urban form, density and microclimate, Build. Res. Inf., 46, 804–808, 2018.

Founda, D. and Santamouris, M.: Synergies between urban heat island and heat waves in Athens (Greece), during an extremely hot summer (2012), Sci. Rep., 7, 1–11, 2017.

Futcher, J. A.: 658-ice tea city, in: 25th Conference on Passve and Low Energy Architecture, 2008.

Giometto, M., Christen, A., Egli, P., Schmid, M., Tooke, R., Coops, N., and Parlange, M.: Effects of trees on mean wind, turbulence and momentum exchange within and above a real urban environment, Adv. Water Resour., 106, 154–168, 2017.

Giometto, M. G., Christen, A., Meneveau, C., Fang, J., Krafczyk, M., and Parlange, M. B.: Spatial characteristics of roughness sublayer mean flow and turbulence over a realistic urban surface, Bound.-Lay. Meteorol., 160, 425–452, 2016.

Gowardhan, A. A., Pardyjak, E. R., Senocak, I., and Brown, M. J.: A CFD-based wind solver for an urban fast response transport and dispersion model, Environ. Fluid Mech., 11, 439–464, 2011.

Grachev, A. A., Andreas, E. L., Fairall, C. W., Guest, P. S., and Persson, P. O. G.: On the turbulent Prandtl number in the stable atmospheric boundary layer, Bound.-Lay. Meteorol., 125, 329–341, 2007.

Grachev, A. A., Andreas, E. L., Fairall, C. W., Guest, P. S., and Persson, P. O. G.: The critical Richardson number and limits of applicability of local similarity theory in the stable boundary layer, Bound.-Lay. Meteorol., 147, 51–82, 2013.

https://doi.org/10.5194/gmd-2019-176
Preprint. Discussion started: 27 August 2019

Grimmond, C. S. B. and Oke, T. R.: Aerodynamic properties of urban areas derived from analysis of surface form, J. Appl. Meteorol., 38, 1262–1292, 1999.

Grimmond, C. S. B., Souch, C., and Hubble, M. D.: Influence of tree cover on summertime surface energy balance fluxes, San Gabriel Valley, Los Angeles, Clim. Res., 6, 45–57, 1996.

Gros, A., Bozonnet, E., and Inard, C.: Cool materials impact at district scale: Coupling building energy and microclimate models, Sustain. Cities Soc., 13, 254–266, 2014.

Gryning, S.-E., Batchvarova, E., Brümmer, B., Jørgensen, H., and Larsen, S.: On the extension of the wind profile over homogeneous terrain beyond the surface boundary layer, Bound.-Lay. Meteorol., 124, 251–268, 2007.

Hamdi, R. and Masson, V.: Inclusion of a drag approach in the town energy balance (TEB) scheme: offline 1D evaluation in a street canyon, J. Appl. Meteorol. Clim., 47, 2627–2644, 2008.

Ho, H. C., Knudby, A., Xu, Y., Hodul, M., and Aminipouri, M.: A comparison of urban heat islands mapped using skin temperature, air temperature, and apparent temperature (Humidex), for the greater Vancouver area, Sci. Total Environ., 544, 929–938, 2016.

Jamei, E., Rajagopalan, P., Seyedmahmoudian, M., and Jamei, Y.: Review on the impact of urban geometry and pedestrian level greening on outdoor thermal comfort, Renew. Sust. Energ. Rev., 54, 1002–1017, 2016.

Kang, W. and Sung, H. J.: Large-scale structures of turbulent flows over an open cavity, J. Fluid Struct., 25, 1318–1333, 2009.

Kastner-Klein, P., Berkowicz, R., and Britter, R.: The influence of street architecture on flow and dispersion in street canyons, Meteorol. Atmos. Phys, 87, 121–131, 2004.

Keck, R.-E., de Maré, M., Churchfield, M. J., Lee, S., Larsen, G., and Aagaard Madsen, H.: On atmospheric stability in the dynamic wake meandering model, Wind Energy, 17, 1689–1710, 2014.

Kikegawa, Y., Genchi, Y., Yoshikado, H., and Kondo, H.: Development of a numerical simulation system toward comprehensive assessments of urban warming countermeasures including their impacts upon the urban buildings' energy-demands, Appl. Energ., 76, 449–466, 2003.

Kleerekoper, L., Van Esch, M., and Salcedo, T. B.: How to make a city climate-proof, addressing the urban heat island effect, Resour. Conserv. Recy., 64, 30–38, 2012.

Kłysik, K. and Fortuniak, K.: Temporal and spatial characteristics of the urban heat island of Łódź, Poland, Atmos. Environ., 33, 3885–3895, 1999.

Kochanski, A., Pardyjak, E., Stoll, R., Gowardhan, A., Brown, M., and Steenburgh, W.: One-way coupling of the WRF–QUIC urban dispersion modeling system, J. Appl. Meteorol. Clim., 54, 2119–2139, 2015.

Kondo, H., Genchi, Y., Kikegawa, Y., Ohashi, Y., Yoshikado, H., and Komiyama, H.: Development of a multi-layer urban canopy model for the analysis of energy consumption in a big city: Structure of the urban canopy model and its basic performance, Bound.-Lay. Meteorol., 116, 395–421, 2005.

Kong, L., Lau, K. K.-L., Yuan, C., Chen, Y., Xu, Y., Ren, C., and Ng, E.: Regulation of outdoor thermal comfort by trees in Hong Kong, Sustain. Cities Soc., 31, 12–25, 2017.

Kono, T., Ashie, Y., and Tamura, T.: Mathematical derivation of spatially-averaged momentum equations for an urban canopy model using underlying concepts of the immersed boundary method, Bound.-Lay. Meteorol., 135, 185–207, 2010.

Krayenhoff, E., Christen, A., Martilli, A., and Oke, T.: A multi-layer radiation model for urban neighbourhoods with trees, Bound.-Lay. Meteorol., 151, 139–178, 2014.

Krayenhoff, E. S.: A multi-layer urban canopy model for neighbourhoods with trees, Ph.D. thesis, University of British Columbia, 2014.

https://doi.org/10.5194/gmd-2019-176
Preprint. Discussion started: 27 August 2019

Krayenhoff, E. S. and Voogt, J. A.: A microscale three-dimensional urban energy balance model for studying surface temperatures, Bound.-Layer Meteorol., 123, 433–461, 2007.

Krayenhoff, E. S., Santiago, J.-L., Martilli, A., Christen, A., and Oke, T. R.: Parametrization of drag and turbulence for urban neighbourhoods with trees, Bound.-Lay. Meteorol., 156, 157–189, 2015.

Kusaka, H., Kondo, H., Kikegawa, Y., and Kimura, F.: A simple single-layer urban canopy model for atmospheric models: comparison with multi-layer and slab models, Bound.-Lay. Meteorol., 101, 329–358, 2001.

Kusaka, H., Hara, M., and Takane, Y.: Urban climate projection by the WRF model at 3-km horizontal grid increment: dynamical downscaling and predicting heat stress in the 2070's August for Tokyo, Osaka, and Nagoya metropolises, J. Meteorol. Soc. Jpn. Ser. II, 90, 47–63, 2012.

Leal Filho, W., Echevarria Icaza, L., Emanche, V., and Quasem Al-Amin, A.: An evidence-based review of impacts, strategies and tools to mitigate urban heat islands, Int. J. Env. Res. Pub. He., 14, 1600, 2017.

Lee, S.-H. and Park, S.-U.: A vegetated urban canopy model for meteorological and environmental modelling, Bound.-Lay. Meteorol., 126, 73–102, 2008.

Lesnikowski, A.: Adaptation to urban heat island effect in Vancouver, BC: A case study in analyzing vulnerability and adaptation opportunities, Ph.D. thesis, University of British Columbia, 2014.

Li, D.: Turbulent Prandtl number in the atmospheric boundary layer-where are we now?, Atmos. Res., 216, 86–105, 2018.

Li, D. and Bou-Zeid, E.: Synergistic interaction between urban heat islands and heat waves: The impact in cities is larger than the sum of its parts, J. Appl. Meteorol. Climatol., 52, 2051–2064, 2013.

Loughner, C. P., Allen, D. J., Zhang, D.-L., Pickering, K. E., Dickerson, R. R., and Landry, L.: Roles of urban tree canopy and buildings in urban heat island effects: Parameterization and preliminary results, J. Appl. Meteorol. Clim., 51, 1775–1793, 2012.

Louis, J.-F.: A parametric model of vertical eddy fluxes in the atmosphere, Bound.-Lay. Meteorol., 17, 187–202, 1979.

Lundquist, K. A., Chow, F. K., and Lundquist, J. K.: An immersed boundary method for the weather research and forecasting model, Mon. Weather Rev., 138, 796–817, 2010.

Mahura, A., Baklanov, A., Petersen, C., Nielsen, N. W., and Amstrup, B.: Verification and Case Studies for Urban Effects in HIRLAM Numerical Weather Forecasting, in: Meteorological and Air Quality Models for Urban Areas, pp. 143–150, Springer, 2009.

Martilli, A. and Santiago, J. L.: CFD simulation of airflow over a regular array of cubes. Part II: analysis of spatial average properties, Bound.-Lay. Meteorol., 122, 635–654, 2007.

Martilli, A., Clappier, A., and Rotach, M. W.: An urban surface exchange parameterisation for mesoscale models, Bound.-Lay. Meteorol., 104, 261–304, 2002.

Masson, V.: A physically-based scheme for the urban energy budget in atmospheric models, Bound.-Lay. Meteorol., 94, 357–397, 2000.

Masson, V., Grimmond, C. S. B., and Oke, T. R.: Evaluation of the town energy balance (TEB) scheme with direct measurements from dry districts in two cities, J. Appl. Meteorol., 41, 1011–1026, 2002.

Masson, V., Gomes, L., Pigeon, G., Liousse, C., Pont, V., Lagouarde, J. P., Voogt, J., Salmond, J., Oke, T. R., Hidalgo, J., Legain, D., Garrouste, O., Lac, C., Connan, O., Briottet, X., Lachérade, S., and Tulet, P.: The Canopy and Aerosol Particles Interactions in TOlouse Urban Layer (CAPITOUL) experiment, Meterol. Atmos. Phys., 102, 135–157, 2008.

Mauree, D., Blond, N., and Clappier, A.: Multi-scale modeling of the urban meteorology: Integration of a new canopy model in the WRF model, Urban Clim., 26, 60–75, 2018.

Mills, G.: An urban canopy-layer climate model, Theor. Appl. Climatol., 57, 229–244, 1997.

https://doi.org/10.5194/gmd-2019-176
Preprint. Discussion started: 27 August 2019

Moeng, C., Dudhia, J., Klemp, J., and Sullivan, P.: Examining two-way grid nesting for large eddy simulation of the PBL using the WRF model, Mon. Weather Rev., 135, 2295–2311, 2007.

Moninger, W. R., Benjamin, S. G., Jamison, B. D., Schlatter, T. W., Smith, T. L., and Szoke, E. J.: Evaluation of regional aircraft observations using TAMDAR, Weather and Forecasting, 25, 627–645, 2010.

Nazarian, N. and Kleissl, J.: Realistic solar heating in urban areas: air exchange and street-canyon ventilation, Build. Environ., 95, 75–93, 2016.

Nazarian, N., Martilli, A., and Kleissl, J.: Impacts of realistic urban heating, Part I: spatial variability of mean flow, turbulent exchange and pollutant dispersion, Bound.-Lay. Meteorol., 166, 367–393, 2018.

Oikonomou, E., Davies, M., Mavrogianni, A., Biddulph, P., Wilkinson, P., and Kolokotroni, M.: Modelling the relative importance of the urban heat island and the thermal quality of dwellings for overheating in London, Build. Environ., 57, 223–238, 2012.

Oke, T., Johnson, G., Steyn, D., and Watson, I.: Simulation of surface urban heat islands under 'ideal'conditions at night Part 2: Diagnosis of causation, Bound.-Lay. Meteorol., 56, 339–358, 1991.

Oke, T. R.: The energetic basis of the urban heat island, Q. J. Roy. Meteor. Soc., 108, 1–24, 1982.

Optis, M., Monahan, A., and Bosveld, F. C.: Limitations and breakdown of Monin–Obukhov similarity theory for wind profile extrapolation under stable stratification, Wind Energy, 19, 1053–1072, 2016.

Palyvos, J.: A survey of wind convection coefficient correlations for building envelope energy systems' modeling, Applied thermal engineering, 28, 801–808, 2008.

Peña, A., Gryning, S.-E., and Mann, J.: On the length-scale of the wind profile, Q. J. Roy. Meteor. Soc., 136, 2119–2131, 2010.

Perret, L. and Savory, E.: Large-scale structures over a single street canyon immersed in an urban-type boundary layer, Bound.-Lay. Meteorol., 148, 111–131, 2013.

Pope, S. B.: Turbulent flows, Cambridge University Press, Cambridge, U.K., 2000.

Rasul, A., Balzter, H., and Smith, C.: Diurnal and seasonal variation of surface urban cool and heat islands in the semi-arid city of Erbil, Iraq, Climate, 4, 42, 2016.

Raupach, M. R., Finnigan, J., and Brunet, Y.: Coherent eddies and turbulence in vegetation canopies: the mixing-layer analogy, in: Bound.-Lay. Meteorol. 25th Anniversary Volume, 1970-1995, pp. 351–382, Springer, 1996.

Redon, E. C., Lemonsu, A., Masson, V., Morille, B., and Musy, M.: Implementation of street trees within the solar radiative exchange parameterization of TEB in SURFEX v8. 0, Geosci. Model Dev., 10, 385–411, 2017.

Resler, J., Krč, P., Belda, M., Juruš, P., Benešová, N., Lopata, J., Vlček, O., Damašková, D., Eben, K., Derbek, P., Maronga, B., and Kanani-Sühring, F.: PALM-USM v1. 0: A new urban surface model integrated into the PALM large-eddy simulation model, Geosci. Model Dev., 10, 3635, 2017.

Rizwan, A. M., Dennis, L. Y., and Chunho, L.: A review on the generation, determination and mitigation of Urban Heat Island, J. Environ. Sci., 20, 120–128, 2008.

Rotach, M. W., Vogt, R., Bernhofer, C., Batchvarova, E., Christen, A., Clappier, A., Feddersen, B., Gryning, S. E., Martucci, G., Mayer, H., Mitev, V., Oke, T. R., Parlow, E., Richner, H., Roth, M., Roulet, Y. A., Ruffieux, D., Salmond, J. A., Schatzmann, M., and Voogt, J. A.: BUBBLE–an Urban boundary layer meteorology project, Theor. Appl. Climatol., 81, 231–261, 2005.

Roth, M.: Review of atmospheric turbulence over cities, Q. J. R. Meteorol. Soc., 126, 941–990, 2000.

Roth, M., Inagaki, A., Sugawara, H., and Kanda, M.: Small-scale spatial variability of turbulence statistics,(co) spectra and turbulent kinetic energy measured over a regular array of cube roughness, Environ. Fluid Mech., 15, 329–348, 2015.

https://doi.org/10.5194/gmd-2019-176
Preprint. Discussion started: 27 August 2019

Geoscientific Model Development Discussions

Runnalls, K. E.: Temporal dynamics of Vancouver's urban heat island, Ph.D. thesis, University of British Columbia, 1995.

Ryu, Y.-H., Baik, J.-J., and Lee, S.-H.: A new single-layer urban canopy model for use in mesoscale atmospheric models, J. Appl. Meteorol. Clim., 50, 1773–1794, 2011.

Salamanca, F., Krpo, A., Martilli, A., and Clappier, A.: A new building energy model coupled with an urban canopy parameterization for urban climate simulations—part I. formulation, verification, and sensitivity analysis of the model, Theor. Appl. Climatol., 99, 331–344, 2010.

Salamanca, F., Georgescu, M., Mahalov, A., Moustaoui, M., and Wang, M.: Anthropogenic heating of the urban environment due to air conditioning, J. Geophys. Res.-Atmos., 119, 5949–5965, 2014.

Salizzoni, P., Marro, M., Soulhac, L., Grosjean, N., and Perkins, R. J.: Turbulent transfer between street canyons and the overlying atmospheric boundary layer, Bound.-Lay. Meteorol., 141, 393–414, 2011.

Saneinejad, S., Moonen, P., Defraeye, T., Derome, D., and Carmeliet, J.: Coupled CFD, radiation and porous media transport model for evaluating evaporative cooling in an urban environment, J. Wind. Eng. Ind. Aerodyn., 104, 455–463, 2012.

Santamouris, M., Papanikolaou, N., Livada, I., Koronakis, I., Georgakis, C., Argiriou, A., and Assimakopoulos, D.: On the impact of urban climate on the energy consumption of buildings, Solar energy, 70, 201–216, 2001.

Santiago, J. L. and Martilli, A.: A dynamic urban canopy parameterization for mesoscale models based on computational fluid dynamics Reynolds-averaged Navier–Stokes microscale simulations, Bound.-Lay. Meteorol., 137, 417–439, 2010.

Santiago, J. L., Krayenhoff, E. S., and Martilli, A.: Flow simulations for simplified urban configurations with microscale distributions of surface thermal forcing, Urban Clim., 9, 115–133, 2014.

Schoetter, R., Masson, V., Bourgeois, A., Pellegrino, M., and Lévy, J.-P.: Parametrisation of the variety of human behaviour related to building energy consumption in the Town Energy Balance (SURFEX-TEB v. 8.2), Geosci. Model Dev., 10, 2801–2831, 2017.

Simón-Moral, A., Santiago, J. L., and Martilli, A.: Effects of Unstable Thermal Stratification on Vertical Fluxes of Heat and Momentum in Urban Areas, Bound.-Lay. Meteorol., 163, 103–121, 2017.

Siu, L. W. and Hart, M. A.: Quantifying urban heat island intensity in Hong Kong SAR, China, Environ. Monit. Assess., 185, 4383–4398, 2013.

Souch, C. and Souch, C.: The effect of trees on summertime below canopy urban climates: a case study Bloomington, Indiana, J. Arboriculture, 19, 303–312, 1993.

Soulhac, L., Salizzoni, P., Cierco, F.-X., and Perkins, R.: The model SIRANE for atmospheric urban pollutant dispersion; part I, presentation of the model, Atmos. Environ., 45, 7379–7395, 2011.

Stull, R.: Practical meteorology: an algebra based survey of atmospheric science, BC Campus, 2016.

Stull, R. B.: An introduction to boundary layer meteorology, Kluwer Academic Publishers, Dordrecht, The Netherlands, 1988.

Sun, J.: Vertical variations of mixing lengths under neutral and stable conditions during CASES-99, J. Appl. Meteorol. Clim., 50, 2030–2041, 2011.

Sun, J., Lenschow, D. H., LeMone, M. A., and Mahrt, L.: The role of large-coherent-eddy transport in the atmospheric surface layer based on CASES-99 observations, Bound.-Lay. Meteorol., 160, 83–111, 2016.

Talbot, C., Bou-Zeid, E., and Smith, J.: Nested mesoscale large-eddy simulations with WRF: performance in real test cases, J. Hydrometeorol., 13, 1421–1441, 2012.

Tseng, Y.-H., Meneveau, C., and Parlange, M. B.: Modeling flow around bluff bodies and predicting urban dispersion using large eddy simulation, Environ. Sci. Technol., 40, 2653–2662, 2006.

https://doi.org/10.5194/gmd-2019-176
Preprint. Discussion started: 27 August 2019

Wang, C., Myint, S., Wang, Z., and Song, J.: Spatio-temporal modeling of the urban heat island in the Phoenix metropolitan area: Land use change implications, Remote Sensing, 8, 185, 2016.

Wang, H., Skamarock, W. C., and Feingold, G.: Evaluation of scalar advection schemes in the Advanced Research WRF model using large-eddy simulations of aerosol-cloud interactions, Mon. Weather Rev., 137, 2547–2558, 2009.

WMO: Aircraft Meteorological Data Relay (AMDAR) Reference Manual, Secretariat of the World Meteorological Organization, 2003.

Wong, M. S., Nichol, J. E., To, P. H., and Wang, J.: A simple method for designation of urban ventilation corridors and its application to urban heat island analysis, Build. Environ., 45, 1880–1889, 2010.

Yaghoobian, N. and Kleissl, J.: Effect of reflective pavements on building energy use, Urban Climate, 2, 25–42, 2012.

Yang, J. and Bou-Zeid, E.: Should Cities Embrace Their Heat Islands as Shields from Extreme Cold?, J. Appl. Meteorol. Clim., 57, 1309–1320, 2018.

Yang, X. and Li, Y.: The impact of building density and building height heterogeneity on average urban albedo and street surface temperature, Build. Environ., 90, 146–156, 2015.

Yang, X., Li, Y., Luo, Z., and Chan, P. W.: The urban cool island phenomenon in a high-rise high-density city and its mechanisms, Int. J. Climatol., 37, 890–904, 2017.

Yuan, C., Norford, L. K., and Ng, E.: A semi-empirical model for the effect of trees on the urban wind environment, Landscape Urban Plan., 168, 84–93, 2017.

Zajic, D., Fernando, H. J. S., Calhoun, R., Princevac, M., Brown, M. J., and Pardyjak, E. R.: Flow and turbulence in an urban canyon, J. Appl. Meteorol. Clim., 50, 203–223, 2011.

Zhang, Y., Li, D., Lin, Z., Santanello Jr, J. A., and Gao, Z.: Development and Evaluation of a Long-Term Data Record of Planetary Boundary Layer Profiles From Aircraft Meteorological Reports, Journal of Geophysical Research: Atmospheres, 124, 2008–2030, 2019.